ADVANCED MATERIALS TECHNOLOGIES
www.advmattechnol.de

Oligonucleotic Probes and Immunosensors Based on Nanoporous Anodic Alumina for Screening of Diseases

*Elisabet Xifre-Perez, Josep Ferre-Borrull, and Lluis F. Marsal**

This paper is an overview of the recent advances in nanoporous anodic alumina sensing platforms based on the interaction of oligonucleotides and antibodies with bioelements (e.g., virus, bacteria, or biomarkers) that can cause or identify diseases. Nanoporous alumina is the common platform material for all these sensing devices that have an enormous potential for the next-generation bioanalytical systems. Nanoporous alumina is a cost-effective material with morphological flexibility that provides high sensitivity to the sensing systems due to its large surface-to-volume ratio. Immunosensors transduce the signal produced by the specific antibody–antigen interaction. They are widely used for clinical analysis due to the high selectivity and sensitivity of their immunoreaction, transduced by different methods (electrochemical, optical, piezoelectric, etc). Another important, outstanding and more recently type of biosensors are based on the oligonucleotic functionalization of nanoporous alumina. Oligonucleotides can bind to a wide variety of elements (small organic molecules, proteins, or cells) with high selectivity, specificity, and affinity, even higher to those of antibodies. The basic concepts and mechanisms of their sensing methods for health care biosensing are introduced. Their transduction methods and great potential applications will be evaluated and classified in detail, together with a discussion of possible future trends.

1. Introduction

The development of sensors for the detection and quantification of bioelements has been object of study for decades. Early detection of disease indicators increases the chances for a successful treatment and recovery, and an adequate and personalized medical therapy depends on its continuous monitoring. However, the current techniques can be time-consuming and usually demand specialized personnel and expensive and sophisticated equipment. Recently, increasingly complex techniques have been developed to achieve a simpler, faster, easier, more sensitive, and highly reliable detection of target analytes. These advances have been carried out in two different aspects. On one hand, the development of innovative bioreceptors, as the use of antibodies has been followed by the outbreaking generation of synthetic oligonucleotides—aptamers—with high binding affinity and selectivity for a specific target. And on the other hand, the improvement of sensing techniques—mainly electrochemical and optical techniques—with the introduction of new elements increasing signal detection, such as metallic layers, nanoparticles, signal probes, and molecular capping. Furthermore, the introduction of nanoporous anodic alumina (NAA) substrates for the development of high-performance sensing platforms has been a wake-up call for the development of extraordinary sensitivity biosensing systems.

This review is aimed at compiling and summarizing the most important advances of NAA biosensors based on antibody–antigen interaction (immunosensors) and complementary oligonucleotides binding. Besides NAA there exist many different approaches to the design and application of oligonucleotides and antibodies (in what is commonly referred to as affinity sensors) on the basis of many other materials such as conducting polymers,[1,2] surface-plasmon resonance (SPR) in thin metallic surfaces and localized surface-plasmon resonance (LSPR) in gold nanoparticle-based systems.[3,4] In the present situation of the COVID-19 pandemic, several reviews extensively survey the different viruses that have historically caused pandemics and the strategies to design and apply affinity biosensors for its detection and diagnostic,[5] and also there exist other useful reviews devoted to describe the efforts on the different techniques used for the generation of a detectable signal upon the reaction of the affinity molecules.[6] Biosensors have been object of several recent reviews, but they are not focused on NAA and most of them evaluate only a specific detection method, i.e., electrochemical sensors,[7–10] optical sensors,[11–13] fluorescence sensors,[14–16] among others. In fact, there is a lack of recent review articles devoted to the application of NAA in the design of affinity biosensors.

In contrast, in this review, we focus for the first time on NAA sensors for the diagnosis and screening of diseases using the two more promising and versatile bioreceptors: antibodies and oligonucleotides. We present a more analytical target-related perspective and evaluate in depth all the successful detection

E. Xifre-Perez, J. Ferre-Borrull, L. F. Marsal
Department of Electric
Electronic and Automatic Engineering
Universitat Rovira i Virgili
Avda. Països Catalans 26, Tarragona 43007, Spain
E-mail: lluis.marsal@urv.cat

The ORCID identification number(s) for the author(s) of this article can be found under https://doi.org/10.1002/admt.202101591.

DOI: 10.1002/admt.202101591

methods for the development of selective and ultrasensitive biosensors. First, we introduce a brief description of the NAA structure and fabrication process as well as its functionalization capabilities. Second, the most relevant and recent biosensing systems developed for the detection and monitoring of disease-related bioelements are described in detail, specially focusing on their sensing principles, performances, and applications. We also highlight in the most recent trends in ultrasensitive detection for each of these sensing principles. Third, a classification of biosensors according to the target analyte is presented. Finally, we conclude this review with a general overview and future perspectives of this exciting and promising research field.

2. Fundamentals of NAA Biosensors

2.1. Fabrication and Technology of NAA

Nanoporous anodic alumina (NAA) (also denominated in literature porous anodic alumina (PAA) or simply porous alumina (PA)) is a material obtained from the electrochemical oxidation of aluminum in acidic electrolytes in the appropriate conditions.[17,18] Electrochemical etching of aluminum is a well-established industrial process since the beginning of twentieth century to provide aluminum with a protective corrosion-resistant oxide layer. In such applications, the obtained oxide layer is compact, hence it is usually designated as a barrier layer. However, in strongly acidic electrolytes at specific concentration and anodization voltage ranges the oxide layer develops pores that grow perpendicular to the aluminum surface.

The most used acids are sulfuric, phosphoric, and oxalic, although many more have been demonstrated such as malonic, tartaric, citric, malic, and even chromic.[19,20] The basic structure of the porous oxide layer is depicted in **Figure 1**. The pores grow from a bulk aluminum surface and in a hexagonal arrangement where each pore has its own hexagonal cell. The pores are surrounded by vertical compact oxide walls and a thin compact oxide layer is also found between the pore interior and the remaining aluminum. This compact layer is generally called a barrier layer. The main geometric characteristics are also depicted on the figure: pore diameter, interpore distance, wall thickness, barrier later thickness, and the total porous oxide layer thickness.

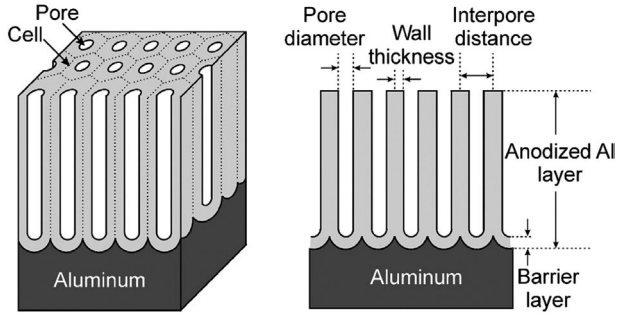

Figure 1. Basic structure of NAA with the characteristic geometrical dimensions. Reproduced with permission.[19] Copyright 2008, Wiley-VCH.

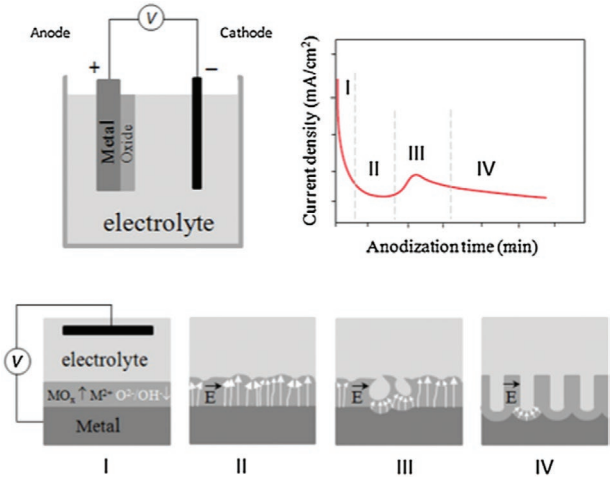

Figure 2. Electrochemical setup and formation mechanism of nanoporous anodic alumina for constant anodization voltage. In phase I, a compact oxide layer is formed, then in phase II oxide thickness inhomogeneities create high electric field regions, which in phase III promote the localized growth of pores that reach a steady growth in phase IV. Reproduced with permission.[21] Copyright 2013, Elsevier.

Different theories have been formulated to explain the formation mechanisms of the porous oxide instead of a compact oxide. The commonly accepted mechanism is depicted in **Figure 2**. The figure depicts the electrochemical cell where the aluminum is used as the anode, while an inert material such as platinum or graphite are used as cathode and a constant anodization potential is applied. In the first stage, a compact oxide layer (barrier layer) grows, increasing the resistance of the electric circuit and producing a drop in current density. The growth of the oxide is driven by the electric field in the barrier layer: the applied anodization potential decays mainly at the oxide, which means that the electric field is very intense. Since the layer is permeable to ions, such an electric field drives oxygen ions from the electrolyte to the oxide–aluminum interface creating new oxide. When this oxide becomes thick enough the flow of ions is reduced, and a stabilization of the current is observed in a second stage of the growth. Since the formed oxide thickness is not uniform, electric field is more intense at the sites where thickness is smaller. This promotes further oxide growth with a concentration of the ion currents at those sites. Such increased currents result in a local temperature increase, promoting oxide dissolution at the oxide–electrolyte interface. These sites become pore nucleation points. In the fourth stage, pores grow steadily with an equilibrium between field-assisted oxide generation rate at the oxide–aluminum interface and heat-assisted oxide dissolution at the oxide–electrolyte interface.

This growth mechanism implies that interpore distance is mainly proportional to anodization voltage,[22–24] as illustrated in **Figure 3**, with weaker dependence on other parameters such as acid concentration and electrolyte temperature. This makes also pore diameter, pore wall thickness, and specially barrier layer thickness proportional to anodization voltage. Pore diameter can then be enlarged by chemical etching usually with a phosphoric acid solution of relatively high concentration and at temperatures between 60 °C and 90 °C.[25,26]

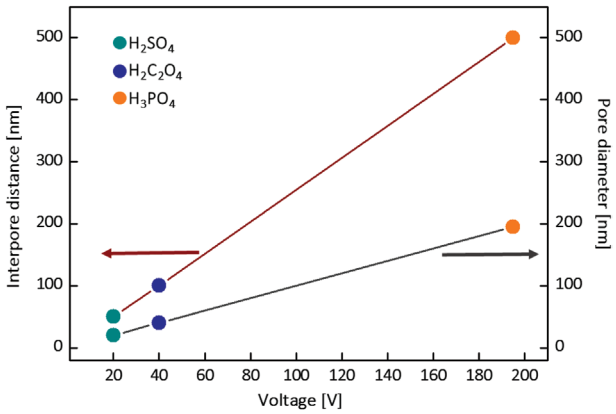

Figure 3. Plot of experimentally obtained interpore distances versus anodization voltage for different experimental conditions.

One of the main breakthroughs in the preparation of NAA was achieved with the two-step anodization method.[27] Pore nucleation sites at the start of anodization happen randomly on the surface, but since the porous oxide represents an expansion of the original aluminum stress appears at the oxide–metal interface. The stress is minimized by a self-arrangement of the pores into a hexagonal pattern. The method proposed by Masuda and Fukuda consisted of a two-step anodization where the first step is conducted for as long as necessary to obtain the self-arrangement, typically about 24 h. Then, this oxide is dissolved leaving a honeycomb pattern of dome-shaped pits on the aluminum that serves as nucleation sites for the second anodization step. Interesting studies on the mechanisms for the self-arrangement have been published.[28,29] Ordering of the pores in a single step has also been obtained by prepatterning the aluminum surface by different methods such as nanoimprint lithography,[30] nanosphere lithography,[31] or optical interference lithography.[32]

The knowledge of the basic formation mechanisms of NAA has led to further development of the technology aiming at structuring the pore geometry with a view to the possible applications. By reducing the anodization voltage by a factor $\sqrt{2}$, interpore distance tends to reduce in the same factor leading to a doubling of the number of the pores, accomplished by a branching of the pores.[33,34] This pore branching strategy has been also applied to remove the barrier layer between the bottom of the pores and the remaining aluminum substrate, thus providing electric contact with the pore interiors.[35–37]

Pore diameter modulation can be accomplished in many ways. First studies employed voltage pulses alternating between the mild and the hard anodization regimes.[23,38] Later, it was demonstrated that a continuous modulation of the applied anodization voltage within the mild anodization regime can lead to a modulation of the pores. Such modulation provides the nanostructures with optical properties. When periodic anodization voltage modulations are applied Distributed Bragg Reflectors are obtained.[39–42] On the other hand, with periodic variation of the anodization current the pore modulation is continuous and rugate filters (also denominated gradient-index filters in the literature) are obtained.[43–45] NAA specular reflection oscillations can be controlled at will by designing the pore geometry, making possible to develop NAA Fabry-Pérot interferometers for smart optical biosensing.[46]

Other strategies for pore diameter modulation consist of alternating different steps of anodization and pore widening or oxide annealing. With subsequent cycles of anodization and pore widening nanofunnels with any desired geometry can be obtained, as long as the diameter decreases with depth.[47,48] In addition, intermediate annealing steps produce changes in the structural crystalline properties of the aluminum oxide that cause a change in the pore widening rate. By including such annealings between the anodization and the pore widening steps are included, inverted nanofunnel structures can be achieved.[49–51] Interesting 3D NAA networks with controlled geometry are obtained with the use of voltage pulses under mild anodization regime and thermal-acidic conditions.[52] Hierarchical NAA substrates with different geometric characteristics are obtained by using an asymmetric two-step anodization process.[53] Different growth regimes (mild and hard), several types of acid electrolytes (phosphoric, oxalic, and sulfuric) and acid electrolyte concentrations, and a range of voltage ratio between the second and the first step of the anodization process are combined in a controlled way to obtain wide range of hierarchical morphologies.

2.2. Functionalization of NAA

The as-produced NAA has a wealth of interesting mechanical, chemical and optical properties, however it is the modification of its surface properties that enables to widely enlarge the scope of applications. Such modification is commonly denominated functionalization and can be classified into two main categories: wet chemical or gas-phase methods. Almost all these methods take advantage of the high density of hydroxyl groups present on the aluminum oxide because of its preparation process, which can be further increased by boiling samples in oxygen peroxide. An extensive review of functionalization techniques can be found in the literature.[21]

One of the most applied surface functionalization techniques in solution is the formation of a self-assembled-monolayer (SAM) of a silane. There exist many silanes such as the 3-aminopropyl-triethoxysilane (APTES) or the pentafluorophenyldimethylpropylchlorosilane (PFPTES), which then can be used to graft other polymers, drugs, or biomolecules.[54–56] This modification can also be combined with other gas-phase routes to provide further optical properties[57] or dual functionalization.[58] Another highly relevant functionalization route is the layer-by-layer (LBL) deposition of polyelectrolytes. This method permits to tune surface properties such as delta potential or electric charge,[59] pore geometry,[60] pore contents such as drugs[61,62] or nanoparticles.[63] Other functionalization routes have also been applied such as electrochemical,[35,36,64–67] gas-phase with thermal vapor deposition,[57,58,68,69] atomic layer deposition (ALD),[70,71] or chemical vapor deposition (CVD).[72–75]

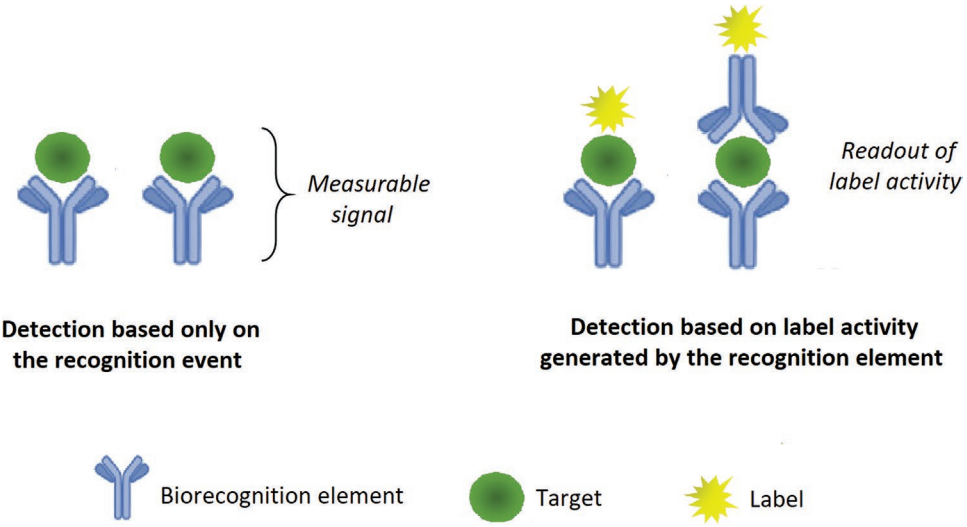

Figure 4. Schematic of the interaction steps for nonlabeled/direct (left) and labeled/indirect immunosensors (right). For labeled/direct immunosensors, the label is generally a fluorescent molecule that can be easily detectable with fluorescence microscopy or confocal microscopy.

2.3. Classification of NAA Biosensors Based on the Bioreceptor

2.3.1. Immunosensors (Antibody–Antigen Interaction)

Immunosensors are high-affinity devices based on the specific and strong interaction between an immobilized antibody and an antigen (analyte).[10] Antibodies are "Y" shape proteins, formed by two heavy and two light polypeptidic chains connected by disulfide bonds, that belong to the immunoglobulins, a family of globular proteins.[76] Antibodies are naturally produced by the immune system as a response to infections caused by viruses, bacteria, fungi, etc., and present a high specific non-covalent interaction with antigens.[77,78] For this reason, antibodies are important biorecognition elements used to target specific analytes for almost four decades.

Immunosensors can be either nonlabeled/direct or labeled/indirect. In nonlabeled/direct immunosensors, the development of the antigen–antibody complex (immunocomplex) produces physical changes that are directly detected by the transducer (**Figure 4**a). In these sensors, the antibody is immobilized on the functionalized NAA substrate to form a sensing device. The surface characteristics of the NAA–antibody template must be sensitive enough to detect the immunocomplex formation. The antigen (analyte) to be detected is deposited on this template and bounds to the complementary antibody from the immunocomplex.[79] This formation alters the physical properties of the surface, such as the optical response, the electrode potential, the transmembrane potential, etc.[80] The principal limitations of nonlabeled immunosensors are the requirements for presenting sufficiently high selectivity and physical properties changes.[79] By contrast, labeled /indirect immunosensors use a detectable label (an enzyme or fluorescent molecule), being the immunocomplex sensitively determined through the measurement of the label (Figure 4b).[81–83,8]

2.3.2. Oligonucleotide-Based Sensors

Another important, outstanding and more recent type of biosensors are based on the oligonucleotic functionalization of NAA. Oligonucleotides are short, single- or double-stranded DNA or RNA molecules[84] that can bind to a wide variety of elements (small organic molecules, proteins, or cells)[85–89] with high selectivity, specificity, and affinity, even higher to those of antibodies.

Generally, oligonucleotide-based sensors use synthesized nucleic acid sequences—called aptamers—as biorecognition element.[90] Aptamers are considered chemical antibodies[91] and are designed to specifically bind selected target molecules. In fact, the name aptamer derives from the Latin word "aptus" that means "fit." Aptamers are obtained with an in vitro generation process called systemic evolution of ligands by EXponential enrichment (SELEX).[92–94] This generation process produces an aptamer with high binding affinity and selectivity for an specific target. These interesting properties of aptamers make them ideal for therapeutic use and for the production of ultrasensitive systems to detect a number of different analytes.

Aptamers present many advantages over antibodies for their use in biosensors. Aptamers are produced in vitro therefore they can be reproduced with high accuracy, can be modified easily, large-scale production is possible and their diversity is very high in comparison to antibodies. Besides, they have easy maintenance as they have a long-term storage at normal conditions and, contrary to antibodies, their denaturation process is reversible. Furthermore, aptamers are much smaller than antibodies, which is important for two reasons: on the one hand, they can access protein epitopes that antibodies cannot access;[95,96] and on the other, the amount of the immobilized target element on NAA for this type of sensor is higher than that for an immunosensor in the same surface area, which results in a linear response range wider than that of an immunosensor.[97]

2.3.3. Others

Although the scope of this review is NAA biosensors based on antibodies and oligonucleotides, other biorecognition elements can be used.

Peptides are one of these biorecognition elements as they bind to several target analytes like proteins, nucleic acids, bacteria, enzymes, or antibodies. Similarly to proteins, peptides are formed by a chain of amino acids, therefore it is possible for peptides with a specific sequence to substitute proteins in biological analysis. Peptides with specific sequences can selectively interact with the target analyte, being suitable for the development of biosensors.

Enzymes have also been used as components in biological analysis and fabrication of novel biosensors. Enzymes are common biocatalysts and the working principle of the biosensors developed with them depends on the catalytic reaction and the binding capability for the target analyte detection. However, the enzyme structure is extremely sensitive, which complicates the use of enzymes for high sensitivity and stability sensors.

3. Classification of the Health Monitoring NAA Biosensors Based on the Detection Method

Several types of detection methods based on the transduction mechanism are used for the development of NAA biosensors. Some of them are used both for immuno- and oligonucleotide-based monitoring and others are characteristic of one of them.

3.1. Voltammetric Sensing

Voltametric sensing is the most widely used detection method for biological analytes. It is a category of electrochemical biosensing as its operating principle relies on the detection of an electrochemical signal, concretely the current is measured as the potential varies. Voltammetric sensors have been used for the detection of oncomarkers, viruses, bacteria, and DNA recognition as they exhibit high sensitivity, selectivity, and capability of detection.[83]

In NAA-based voltammetric sensors, an NAA membrane is the base of the sensing platform, the pores of which are used as artificial nanochannels with a similar structure and ion transmission characteristics to biological ion channels. Besides, these NAA ion channels can be easily functionalized with biorecognition molecules and provide a confined environment with signal amplification, ideal for biological detection. For voltammetric measurements, the functionalized NAA membrane is placed in the middle of two cells containing the same volume and concentration of electrolyte solution (**Figure 5**). The Ag/AgCl electrodes are used to record the I–U curve under bias in linear scan voltage mode. This detection method has demonstrated extraordinary selectivity and sensitivity at picomolar and femtomolar levels[98] in macromolecule target detection when attaching aptamers or antibodies to the nanopores of the NAA membrane. The confined space in the nanopores highly influences on the mass transfer across these nanochannels when the target analyte interacts with the biorecognition element. The biorecognition element–target analyte union produces an immunoreaction inside the pores of the NAA membranes that allows the formation of immunocomplexes. These immunocomplexes produce a partial blocking effect inside the pores and influence the diffusion of electroactive species inside them

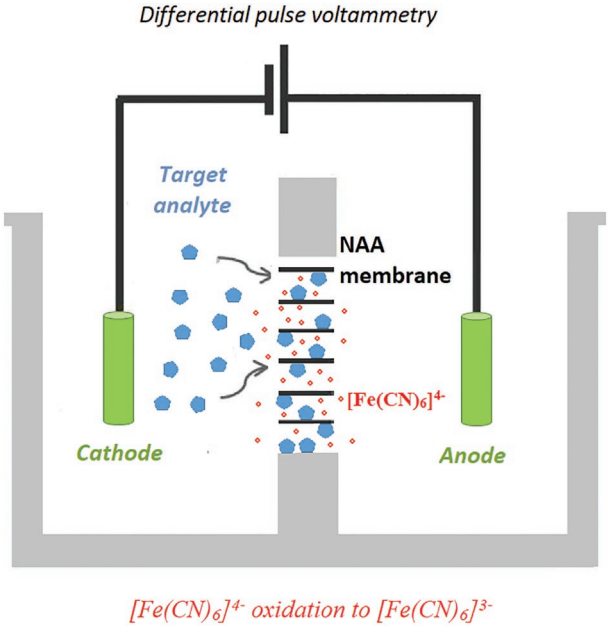

Figure 5. Schematic of the generic detection system and principle for NAA-based voltammetric sensors.

resulting in a decrease in the voltammetric signal of $[Fe(CN)_6]^{4-}$ oxidation to $[Fe(CN)_6]^{3-}$. As a result, the voltammetric peak current corresponding to the oxidation of $[Fe(CN)_6]^{4-}$ to $[Fe(CN)_6]^{3-}$is used as the detection signal.[99] However, the biorecognition event produces a moderate occupancy/blocking of the nanochannels. To increase this occupancy and therefore to enhance the sensitivity of the detection platforms, the use of nanoparticles has been introduced. Nanoparticles are small enough to enter into the nanopores and produce an additional blocking effect to the biorecognition event.

A simple bare NAA membrane with antibody attaching has been reported to be a rapid and high sensitivity and selectivity platform for analyte detection. It has been used for the detection of bacterial hyaluronidase in *Staphylococcus aureus* bacteria,[100] *Escherichia coli* bacteria,[101] dengue virus,[102] West Nile virus,[103] and exosomes,[104] by attaching one or two antibodies to the NAA substrate. Instead of antibodies, aptamers have also been immobilized on this very simple sensing platform consisting of an NAA membrane frequently sputtered with gold, for example for the detection of listeria monocytogenes bacteria,[105] potassium and adenosine triphosphate,[106] lead,[107] and thrombin,[99] although aptamer-based voltammetric sensors generally use additional elements for signal enhancement, like nanoparticles. Despite the great importance of NAA pore diameter in voltammetric sensors, the number of works that analyze the influence of the pore size on the detection efficiency is very small. Zhou et al.[105] evaluate the efficiency of the detection system for *Listeria monocytogenes* bacteria for NAA pore diameters 20, 100, and 200 nm, deducing that 20 nm is the best diameter for the optimal performance of the sensor because of its higher specific area, and therefore the higher density of aptamer. This same work also evaluates the specificity of the developed sensor for *Listeria monocytogenes* with the additional presence of *Staphylococcus aureus* or *Escherichia coli*. Yu et al.[106] also

fabricate NAA sensing substrates with different pore diameters (25, 55, and 90 nm) to design their potassium and adenosine triphosphate detector with the most efficient response. In this case, 25 nm diameter was deduced to be the most suitable size for their detection system. Finally, Chen et al.[107] evaluate their detection experiments for 20, 50, 100, and 200 nm nanochannels, being the 20 nm diameter nanochannels the ones with the best detection response. The results presented by these authors clearly indicate that the diameter of the nanochannels is really decisive for the quality and sensitivity of the resulting sensing devices, and that narrower pore sizes optimize the performance of voltammetric immunosensors.

The sensitivity of the voltammetric systems has been demonstrated to be improved with the use of nanoparticles with diameters small enough to enter inside the NAA pores for a more efficient blocking. An interesting application of voltammetry with nanoparticles is reported by Jiang et al.[108] for the detection of microRNAs (miRNAs), important for early cancer diagnosis.[109] A bivalent recognition using SiO_2 nanoparticles produces the blocking of the NAA pores and therefore the amplification of the signal. The bivalent recognition is performed with two oligonucleotides that individually contain the complementary sequence for opposite ends of the target miRNA. One oligonucleotide is attached to the NAA pores and the other is linked to the nanoparticles. A detection limit of 31×10^{-18} M is reported. However, SiO_2 is not the most extended material for voltammetry nanoparticles. Gold is the commonly used material for these nanoparticles, due to its easy functionalization characteristics. Gold nanoparticles (AuNP) have been used in aptamer-based sensing platforms for the detection of DNA[110] and thrombin.[111] **Figure 6** clearly indicates the sensing principle with the use of AuNP.

Interestingly, NAA nanochannel diameters used in voltammetric systems with nanoparticles are required to be considerably wider than that for traditional voltammetric systems. As explained before, traditional voltammetric systems are demonstrated to optimize their performance with nanochannels diameters mostly around 20 nm [100,104–107] and reaching exceptionally 50 nm.[99,102] On the contrary, when using nanoparticles for sensitivity improvement, the diameter of the NAA pores generally used is around 200 nm[108,110,111] as the nanoparticles are needed to enter inside the nanochannels and partially block them for signal amplification.

The enhanced response of the biosensors using AuNPs is improved by depositing silver onto the surface of the AuNP in the work of Escosura-Muñiz and Merkoçi[112] for the detection of cancer biomarkers. Pan et al.[98] developed an aptamer-based biosensor for the femtomolar detection of Mucin 1, an epithelial cancer marker. Different from other works, the aptamer is immobilized onto the AuNP and the AuNPs do not enter inside the pores, they are subsequently deposited on the NAA membrane. A multilayer deposition of aptamer-modified gold nanoparticles on the NAA membrane produces an increase of the signal and improves de sensitivity of the biosensor with a limit of detection of 0.0364 fg mL^{-1} (0.0025×10^{-18} M).

A gold layer deposited on the NAA membrane instead of AuNPs has been used by Rajeev et al.[113] for a sensitive and rapid detection of Flightless I (Flii) protein, a biomarker of wound chronicity. In this work, different NAA pore diameters (45, 65, and 100 nm) were evaluated for the efficiently binding of Flii conjugate to the bioreceptors within the nanochannels. The highest sensitivity was demonstrated for 65 nm pores. The same research group detected this same biomarker introducing magnetic nanoparticles as signal enhancers for the sensing platform.[114]

3.2. Impedimetric Sensing

Impedimetric sensors are another type of electrochemical sensors based in this case on electrochemical impedance

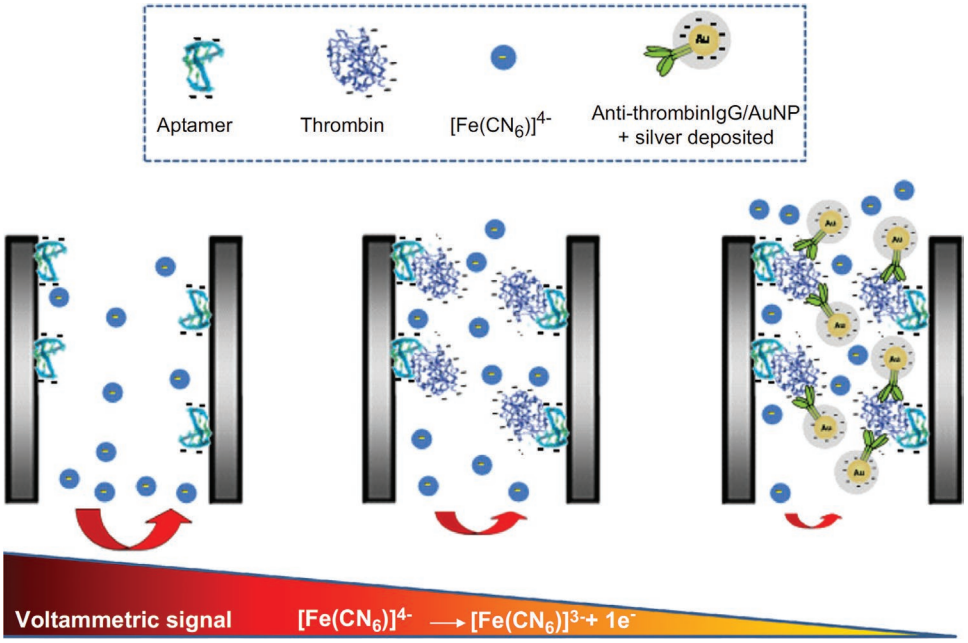

Figure 6. Thrombin detection process in a voltammetric NAA-based sensor using AuNAP. Reproduced with permission.[111] Copyright 2013, Elsevier.

spectroscopy (EIS), a technique that applies a small amplitude alternating current signal over a wide range of frequencies to measure the impedance characteristics of a cell. The setup for EIS measurements is very similar to that for voltammetric sensors but in this case electrical impedance is the monitoring signal proportional to analyte recognition activity.[115,7]

Impedance measurements are the most widely used for the monitoring of antibody–antigen interactions. *Escherichia coli* bacteria are the most detected target analyte.[116–119] An ultrasensitive *E. coli* immunosensor has been presented by Chan et al.,[119] using magnetic beads to enhance the sensitivity of the NAA platform. The *E. coli* conjugated magnetic beads are concentrated in a small region of the antibody immobilized NAA membrane with a magnet (**Figure 7**), producing a long interaction time and a high concentration of bacteria on the NAA membrane that enhances the sensitivity of the sensor (LOD 10 CFU mL^{-1}).

Other bacteria like *Staphylococcus*[118] or *Salmonella*,[120] inflammatory and cardiovascular biomarkers like C-reactive protein and myeloperoxidase),[121] viruses like Dengue,[122] and allergens like histamine[123] have also been detected by immobilizing antibodies onto NAA membranes. The study of the *Salmonella* bacteria immobilization on NAA membranes[120] is also extended to evaluate the bacterial response to antibiotics, concretely to enrofloxacin and ampicillin, with a concentration of 0.1×10^{-9} M. For the detection of histamine Ye et al.[123] also used magnetic nanoparticles for signal amplification.

Aptamer-based impedimetric sensors have also been developed more recently. An ultrasensitive impedimetric system conjugating an NAA membrane with AuNPs was developed by Ye et al. for the detection of *E. coli* (LOD of 100×10^{-12} M).[124] The same system was used by Peinetti et al. for the monitoring of Adenosine monophosphate (a molecule involved in different neural processes in the brain like sleep, arousal, and locomotion),[125] and DNA strands.[126] The immobilization of DNA on aptamer-modified NAA membranes was also monitored by Wu et al.[127] and Ye et al.[128] The selectivity of impedimetric platforms is demonstrated in the study of Gosai et al.[129] where α-thrombin is detected with a LOD 10×10^{-12} M with the interfering presence of a high concentration (500×10^{-6} M) of human albumin serum. Aptasensors for Dengue virus detection have also been developed using aptamers for the biorecognition.[130,131] The work reported by Deng et al.[130] detects the target Dengue DNA for a concentration range of 10^{-12} to 10^{-6} M. The same NAA platform was used for the detection of *Legionella pneumophila* DNA, achieving a detection limit of 3.1×10^{-13} M for the working range of a 10^{-13} to 10^{-6} M.[132]

The NAA substrates reported for impedimetric detection present a wide variety of pore sizes, although wide diameter pores (>100 nm) are generally used.[118,120,122,123,130] Ye et al.[124] study the effect of the NAA pore size on the quality and sensitivity of their *E. coli* detection system. Pore diameters of 20, 50, and 100 nm are evaluated, being the100 nm pore sensor the one with the lowest limit of detection and highest detection sensitivity. In this work, gold nanoparticles are used for signal amplification, therefore the good efficiency is attributed to the major quantity of nanoparticles entering into the NAA pores.

3.3. Fluorescence Spectroscopy Detection

Fluorescence spectroscopy is an optical and traditional method widely used for developing sensing systems. To better understand the principles of this detection method, we have to understand the concepts involved. Luminescence is the phenomenon by which light is produced through excitation, with no temperature increase. Fluorescence is defined as "a short-lived type of luminescence created by electromagnetic excitation which is generated when a substance absorbs light energy at a short (higher energy) wavelength and then emits light energy at a longer (lower energy) wavelength."[14]

For fluorescence detection, a fluorescent reporter (fluorophore) is generally used. A fluorophore is a molecule that can display fluorescence. Fluorophores are characterized by their absorbance and emission spectrum. The specific wavelength at which fluorophores present an efficient absorption of energy is the peak absorbance. And the peak emission is the specific wavelength at which they most efficiently emit the energy. The wavelength range for the peak absorbance is shorter than that for the peak emission, and both of them conform the definition of the fluorophore.

In single fluorescence event detection, when the target analyte binds to the functionalized NAA substrate, their interaction produces a change in the fluorescence emitted by the fluorophore, that can be observed or measured by fluorescence microscopy or confocal scanning laser microscopy.

Several strategies in single fluorescence detection are reported using NAA as the detection platform.[133–135] NAA fluorescence immunosensors have been developed for the detection and quantification of immunoglobulins.[134,135] Also, a high sensitive platform for the detection of galectins—an excellent biomarker for tumor diagnostics and monitoring—was developed by Hattum et al.[136] Specific antibodies selective to galectin-1 and galectin-9 were immobilized onto the NAA substrate (**Figure 8**a). Subsequently, galectins were captured from

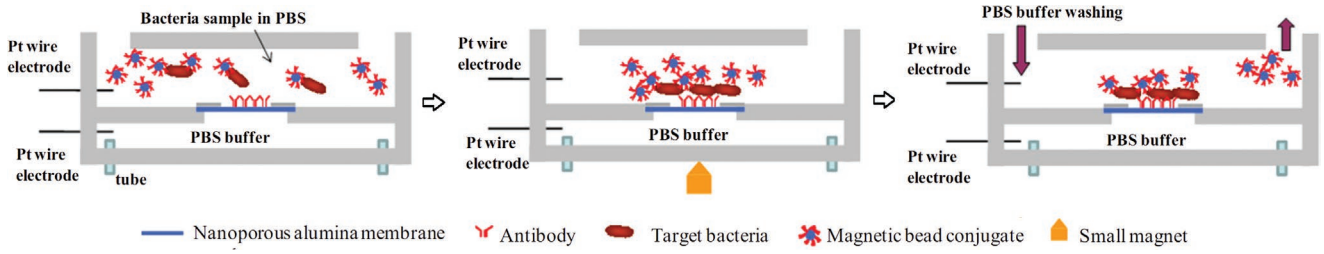

Figure 7. Impedimetric immunosensor process using magnetic nanoparticles. Adapted with permission.[119] Copyright 2013, Elsevier.

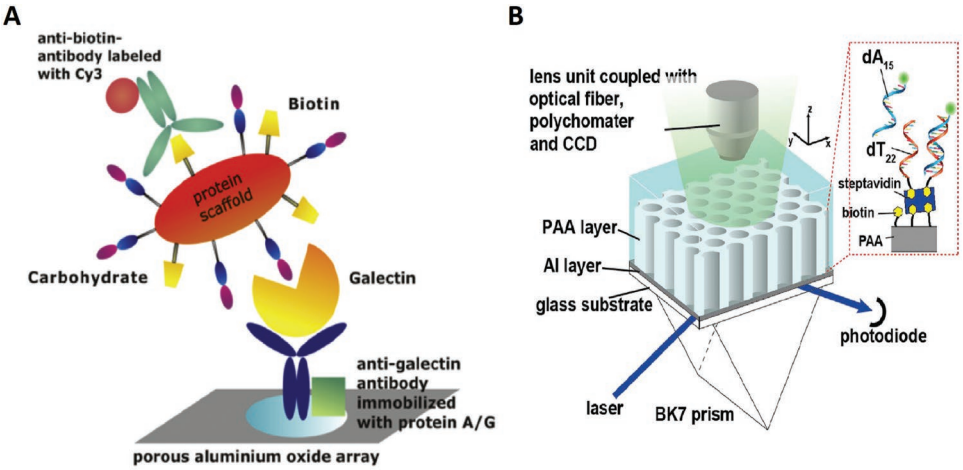

Figure 8. A) Fluorescence detection process of exosomes. Adapted with permission.[136] Copyright 2013, Elsevier. B) Schematic of a waveguide aptasensor. Adapted with permission.[137] Copyright 2014, AIP Publishing.

cell lysate and bound by the general ligand, which was then visualized by a fluorescently labeled antibiotin antibody. This system allowed the detection of galectin quantities with a LOD of 4 ng in *E. coli*-spiked cell lysates.

NAA is also used for developing fluorescence sensing platforms using aptamers. Fan et al. proposed an aptasensor for the real-time monitoring of DNA hybridization.[137] In this case, the NAA layer and its aluminum base are used as a waveguide (Figure 8b). Biotinylated dT_{22} was used as the probe strand, with a complementary target DNA strand of dA_{15} and a non-complementary target strand of dT_{15}. The target strands dA_{15} and dT_{15} were labeled with a fluorophore and the hybridization process was measured based on the time-dependent fluorescence signal.

Fluorescence is also the detection method reported in the aptasensor developed by Aramesh et al.[138] A NAA membrane with a coating of diamond-like carbon is used here for the development of a sensor for highly sensitive and selective detection of cancer oncomarker RAK I, a common 21-mer biomarker in patients with prostate, breast, and gynecological cancer.

Another type of fluorescence-based biosensors is developed using two fluorophores instead of a single one. This is the case of the NAA aptasensor developed for the detection of the Ebola virus.[139] This system was designed based on the principle of Förster resonance energy transfer (FRET) that involves a donor and an acceptor fluorophore pair (**Figure 9**). In this work, BaGdF5:Yb/Er upconversion nanoparticles (UCNPs) were conjugated to oligonucleotide probes and deposited on the NAA membrane. In parallel, AuNP were linked to target Ebola virus oligonucleotide. The hybridization process between the Ebola target and the probe oligonucleotides causes close proximity of UCNPs and the AuNP (donor and acceptor) on the NAA membrane. The use of NAA membranes for this donor and acceptor reaction improves the detection limit from picomolar to femtomolar levels.

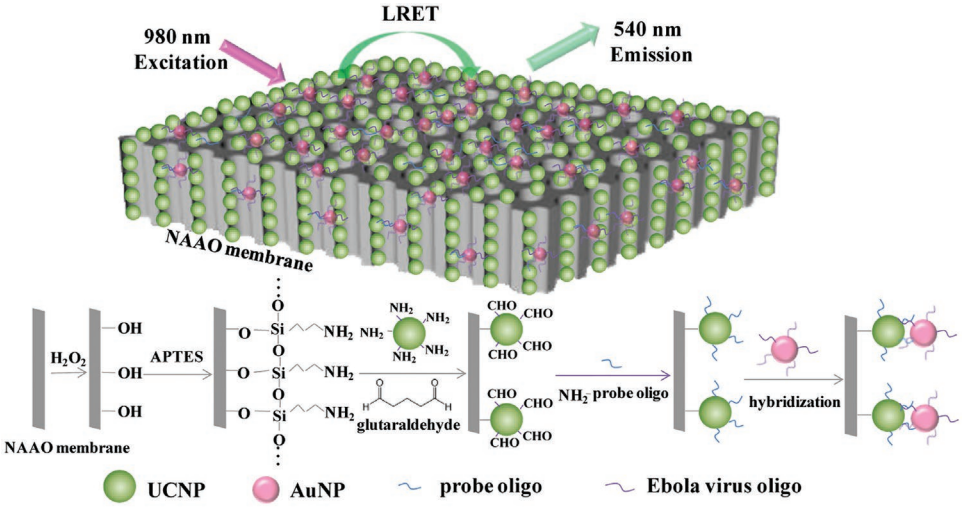

Figure 9. Donor–acceptor reaction for the detection of Ebola virus. Reproduced with permission.[139] Copyright 2016, American Chemical Society.

In general, the NAA substrates used for fluorescence detection present pore diameters in the range from 150 to 200 nm.[133–135,138]

3.3.1. Molecular Gate Based Sensing

Although in molecular gate-based biosensors the detection method evaluates the light emission from a fluorophore, this innovative type of aptamer-based biosensors deserves a separate explanation from the ones presented in the fluorescence sensing section.

The difference here resides in the biorecognition process, completely different from the rest of fluorescence spectroscopy detectors. In molecular gate-based sensors, an NAA support is loaded with a fluorescent reporter (generally rhodamine B), then the pores are capped with an aptamer-based gating mechanism so that the fluorophore is released by the presence of the target analyte (**Figure 10**).

These gated sensor systems have been recently developed by the research group of Martínez-Máñez using NAA as material support.[140–143] Although the concept of gated materials was introduced some years before, especially for developing drug delivery systems,[144–146] the few sensing applications reported used mesoporous silica nanoparticles as base material.[147–149] NAA substrates have the same reservoir advantages than mesoporous silica but do not present the important disadvantages of nanoparticles: difficult handling, harmful if inhaled or deposited on skin, and nonuniform suspensions that make it difficult to develop highly reproducible sensing systems. Besides, NAA is biocompatible, with easy functionalization and handling properties and its pores are perfect nanocontainers with high load capacity. A special characteristic of the NAA substrates used for molecular-gated detection systems is their pore diameter, extremely small, from 5 to 8 nm. No other sensing principle uses pore diameters lower than 20 nm. The reason for these exceptional narrow NAA channels is basically the detection principle: the pores are capped with oligonucleotide sequences and therefore their entrance must be minimized.

The gated NAA sensing system developed by the group of Martínez-Máñez was first applied to the successful detection of cocaine.[140] The NAA support was capped with a specific oligonucleotide sequence capable of recognizing cocaine. With the presence of an aqueous solution of cocaine, the rhodamine B loaded inside the NAA pores was released. The selectivity of the system, with a LOD of 5×10^{-7} M, was assessed using heroin and morphine drugs. The real applicability of the NAA sensing support was also evaluated in a competitive matrix, such as saliva. The NAA support developed for the gated sensing was stable, did not degrade in aqueous solutions, and could be calcined and reused several times, reducing the cost of the sensing process.

In addition to cocaine, this gated NAA detection system has been successfully used for the monitoring of bacteria (*Staphylococcus aureus*,[150] mycoplasma,[143]]) fungus (*Candida auris*,[141] *Candida albicans*,[142] *Pneumocystis pneumonia*[151]), biomarkers,[152,153] and allergenic proteins.[154]

3.4. Reflectometric Interference Spectroscopy (RIfS) Detection

Reflectometric interference spectroscopy (RIfS) is an optical sensing technique based on the white-light interference in thin films.[155] NAA is a very advantageous nanostructured material for RIfS detection as its reflectance spectrum presents oscillations with well-defined peaks generated by the Fabry–Pérot effect[156] and a very high surface area for capturing analytes. These interesting characteristics of NAA are the basis of high sensitivity RIfS-based sensors.[157]

The detection principle of RIfS sensors is based on the refractive index variation, i.e., the effective refractive index of the NAA substrate is modified by the binding of the target analyte.[158] A typical RIfS set-up for the detection of target analytes is presented in **Figure 11**. The NAA substrate is generally placed in a flow system. The fluid with the dissolved

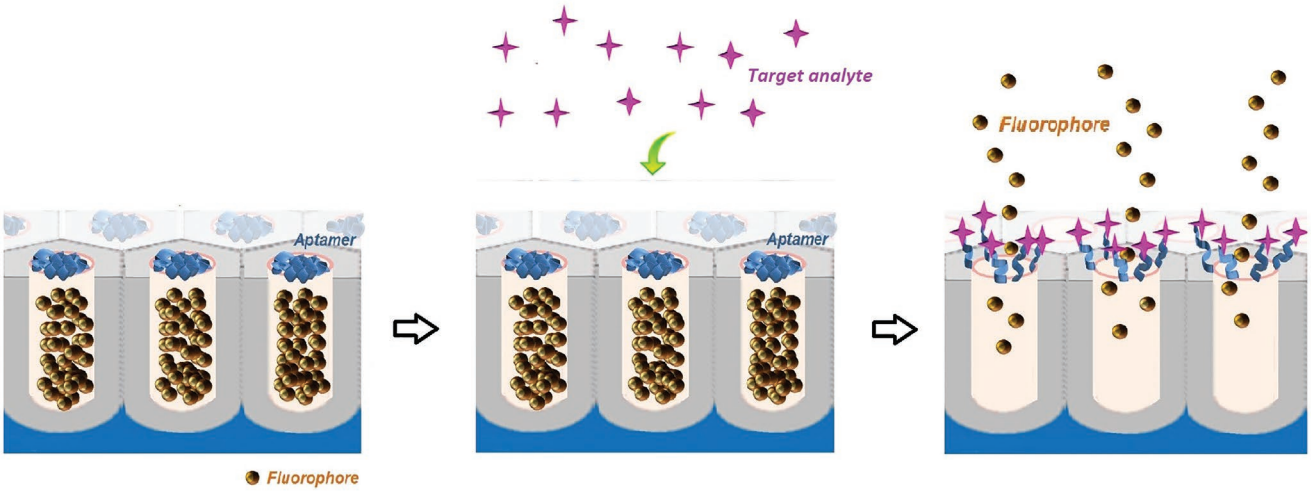

Figure 10. Schematic of the molecular gate sensing process: the NAA pores are initially loaded with a fluorophore and blocked with an aptamer or other oligonucleotide, the so called molecular gate (left). With the presence of the target analyte, the molecular gate interacts with the target, leaves the pores open and then the fluorophore is released (right).

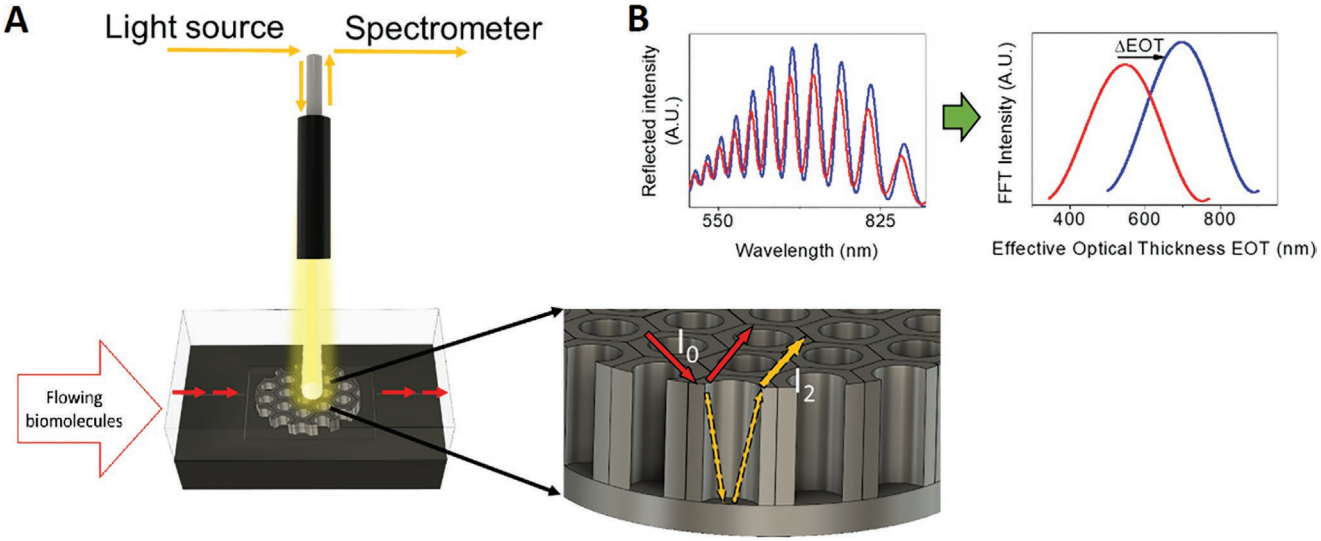

Figure 11. A) Optical system and detection principle schematic for RIfS detection. The principle is represented for NAA substrates showing the interaction of the light reflection on the surface and bottom of the NAA pores. B) RIfS spectrum measured by Pol et al. with this RIfS-NAA platform used to detect different levels of thrombin. The measured reflectance spectrum before (red) and after (blue) the thrombin binding to the NAA pores are mathematically processed (FFT) quantitatively indicating the thrombin concentration by the ΔEOT value. Adapted with permission.[68] Copyright 2019, MDPI.

target analyte is pumped through the cell, and when in contact with the adequately functionalized NAA pores, interacts and the binding of the analyte to the walls and surface of the NAA pores produces a variation of the NAA effective refractive index (n_{eff}). The binding event is monitored in real time and in situ using a white light source directly illuminating the NAA layer. The reflection spectrum of this light from the NAA layer follows a thin-film interference spectral pattern, generated by the light reflecting from the fluid–NAA and the NAA–aluminum interfaces. The wavelengths of the spectral fringe maxima in the interference spectrum meets the Fabry–Perot relationship:

$$m\lambda = 2n_{\text{eff}}L = \text{EOT} \tag{1}$$

where λ is the wavelength of the spectral fringe maximum of order m, n_{eff} is the effective refractive index of the NAA layer, L is the pore length, and EOT is the effective optical thickness.

The Fourier transform of the reflectance spectrum is a single peak whose x-axis position corresponds to the EOT of the NAA layer.[159]

In the last decade, the performance of RIfS systems as a sensing platform has improved and its use has considerably increased for performing highly sensitive, rapid-response, label-free, qualitative, and quantitative detection of several bioelements like amino acid molecules,[160] environment monitoring, and drug release.[161] The NAA substrates used for RIfS detection have pore diameters in the range from 30 to 70 nm.[68,162–168]

NAA-RIfS technology has been used by Rajeev et al.[162] to develop an immunosensor for the detection of tumor necrosis factor-alpha (TNF-α), a proinflammatory cytokine important to wound healing. The detection substrate consisted of an NAA layer (different pore diameters were assessed) sputter-coated with a thin layer of Pt and chemically functionalized via silanization for the covalent bound of anti-human TNF-α antibody on the pores surface (**Figure 12**a). The selective binding of the protein was monitored in real time with the evaluation of the EOT change (Figure 12b). A linear response of the detection system with a limit of detection of 0.13 μg mL^{-1} is reported.

Another NAA-based immunosensor was reported by Kumeria et al.[163] for the detection of circulating tumor cells, specially important for monitoring the treatment of cancer during the initial stages of metastatic disease.[169,170] The NAA substrate was gold-capped and functionalized with a biotinylated anti-EpCAM antibody. Their results demonstrate the direct detection in less than 5 min of cancer cells concentrations between 1000 and 100.000 cells mL^{-1} in PBS buffer solution and in diluted blood samples.

RIFS technology has also been applied for the development of aptamer-based sensors. Pol et al.[68] developed an aptamer-based sensor with an NAA-RIfS system. In this work, thrombin binding aptamer was immobilized onto the inner surface of NAA pores (5 μm depth and 30 nm pore diameter) through streptavidin–biotin interaction. The NAA-RIfS system demonstrated the high specificity and capacity to detect thrombin in the $\times 10^{-6}$ M range with a limit of detection of 7.2×10^{-9} M and a sensitivity of 45.5 nm μM^{-1}.

More recently, aptamer-based detection with NAA-RIfS systems has been used for the monitoring of other harmful substances in blood. One of them is salicylic acid (SA), whose concentrations can cause health problems like urticaria, angioedema, rhinitis, and asthma to hypersensitive people.[171] In the study of Chen et al.,[172] five different aptamers for SA are developed and their binding capability is assessed. The biosensor developed presented a detection limit of 0.1×10^{-6} M of SA in buffer, significantly lower than the antibody-based detection reported.[173] Another is the work developed by Feng et al.[164] that detects theophylline (TP), a drug used for the treatment of respiratory diseases that must be quickly and regularly monitored in current clinical practice since it becomes toxic at high

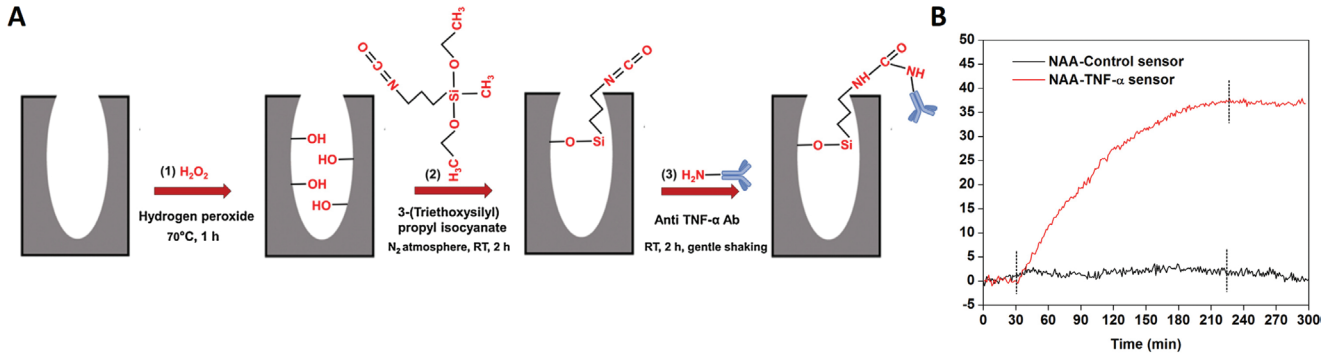

Figure 12. NAA-RIfS immunosensor for the detection of TNF-α. A) Surface modification of the NAA substrate. B) Sensing response. Adapted with permission.[162] Copyright 2018, Elsevier.

concentrations and can be lethal or lead to permanent neurological damage.[174] NAA-based RIFS spectroscopy has also been used for the accurate determination in real time of DNA hybridization[165] its melting temperature (T_m).[166]

In addition to all the mentioned applications, a NAA-RIFs innovative strategy for sensitivity enhancement has been developed by introducing some differences in the analysis of the interferometric reflectance spectrum.[167,168,175,176] Similarly to the traditional RIfS, the reflectance spectrum is measured with a fiber optic spectrometer and presents well-defined peaks generated by the Fabry–Pérot effect. However, the intensity and the area of one peak of the spectrum are evaluated for detection, instead of the traditional variation of the EOT. The reason for this is the use of a signal probe, usually methylene blue (MB), that has demonstrated high ability to interact with DNA.[177,178] The MB probe increases the photonic response of the traditional system during the aptamer–target interaction resulting in high analytical performance sensors. This innovative method is developed by Tabrizi et al. for the detection of *Salmonella*-specific DNA fragment.[167] In this work, a single-strand DNA (ssDNAsal) probe that presents high affinity to *Salmonella*-specific DNA fragment was attached to the NAA surface (**Figure 13**). The interaction of different concentrations of *Salmonella*-specific DNA fragment with the DNA probe is detected with a shift of the interference spectrum, but the subsequent intercalation of MB into the complex produces not only a higher shift of the interference spectrum but also a very significant variation of the reflected light intensity. The authors report a limit of detection of 0.01×10^{-9} M for the concentration range $0.25–50.0 \times 10^{-9}$ M. The selectivity of the sensor was assessed with the use of *Staphylococcus aureus*-specific DNA fragment and *Escherichia coli*-specific DNA fragment.

A similar method is used for the detection of amyloid β oligomers, Alzheimer's disease biomarkers.[168] In this case, the aptamer was first attached to the NAA pores walls, and then methylene blue (MB) was immobilized into the aptamer as the photo-probe, generating the MB/G-quadruplex complex. In contact with the Aβ oligomers, the MB/quadruplex complex broke and MB was released from the sensing substrate. A good response to the concentration of Aβ oligomers in the range of 0.5–50.0 $\mu g \times mL^{-1}$ and a detection limit of 0.02 $\mu g \times mL^{-1}$ (at $3\sigma/S$) is reported for this sensing structure.

3.5. Localized Surface Plasmon Resonance (LSPR)

Interest in surface plasmon resonance (SPR) biosensors for real-time and in situ monitoring of analyte–receptor binding has grown exponentially since the first publications in the seventies. In SPR systems, surface plasmons are generated from an evanescent electromagnetic wave, which is produced by a light beam focused on the surface of a prism coated with a thin metallic film.[179]

Similarly, but more affordable and accessible than SPR, localized surface plasmon resonance (LSPR) has been used for the development of label-free high sensitivity biosensors. Traditional SPR uses a continuous gold film, while LSPR is produced by metal nanoparticles, usually silver and gold. For LSPR less complex equipment is necessary as no prism is required. In LSPR, a powerful resonance absorbance peak is produced in the visible range of light. For detection, the position of this peak is analyzed, being quite sensitive to the local refractive index around the particle.

Both antigen–antibody and aptamer–target molecule interactions can be rapidly and cost-effectively monitored with LSPR, a technique that has been successfully used for label-free and quantitative detection in clinical, environmental, and food analysis applications.[158,180]

For LSPR, gold-capped NAA substrates have been successfully used for high sensitivity and specific monitoring of the bioreceptor–target analyte interaction. Furthermore, an increase of the sensitivity for LSPR-NAA biosensors has been achieved by using a combination of LSPR technique with interferometry in the relative reflected intensity (RRI) spectrum. One of these LSPR-interferometry immunosensors is reported by Yeom et al.[181] for a real-time detection of the human C-reactive protein (CRP), a blood serum marker for infections and inflammatory processes. The detection substrate consists of a NAA layer, with 1 µm length pores, covered by e-beam evaporation with a 5 nm thick Ni layer and a 15 nm thick Au layer. Then, the CRP antibody is immobilized on its surface to conform the sensor chip. The CRP antigen dilution flows on this substrate in a controlled way with a flow chamber and a micropump. The monitoring is performed using a white-light source emerging from an optical fiber bundle to perpendicularly illuminate the substrate. The reflected light is collected by the detection fiber probe with the same bundle and measured with a spectrometer.

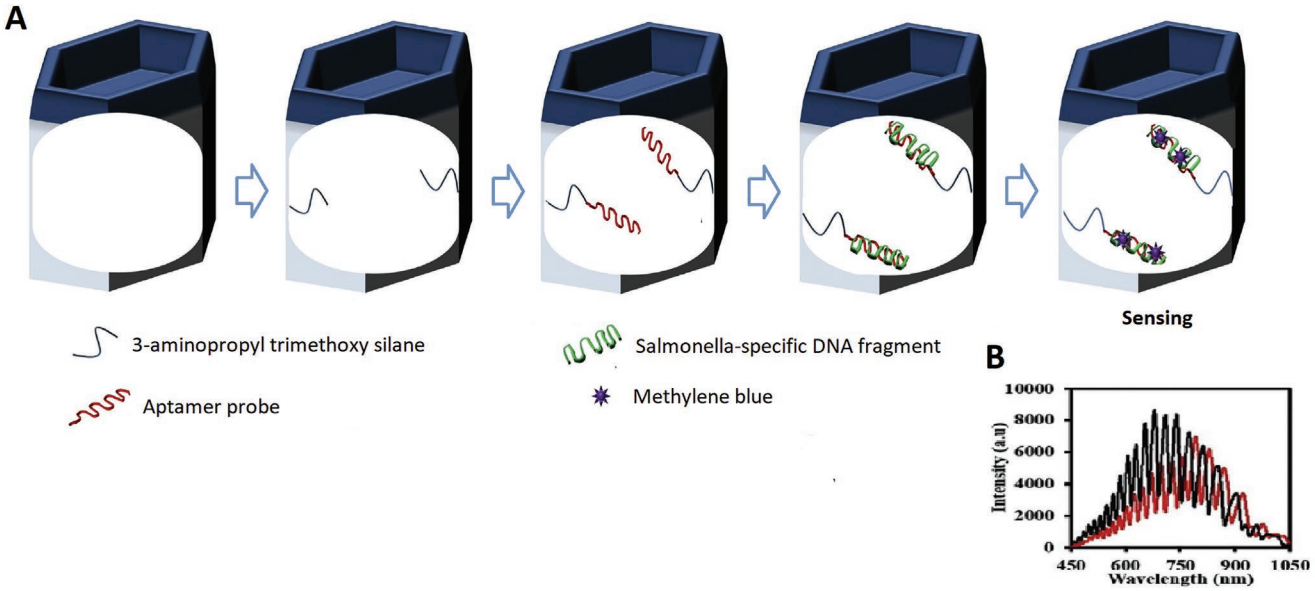

Figure 13. Innovative RIfS-based detection process using NAA substrates for the detection of *Salmonella*. A) Schematic of the pore surface functionalization and target binding. In this case, MB is used at the final step as signal probe. B) Interferometric reflectance spectrum obtained before (black) and after (red) the target binding to the pores. Adapted with permission.[167] Copyright 2020, Elsevier.

The wavelength range analyzed was 680 to 730 nm. With the antigen-antibody binding, changes in the refractive index of the substrate are induced, which are detected as changes of its reflectivity. This sensor chip system is reported to present a high selectivity, and sensitivity of ≈1 fg mL^{-1}.

Another type of immunosensor LSPR-based was developed by Lv et al.[183] for the detection of exosomes, novel biomarkers for the monitoring and prediction cancer diseases.[184] In this case, NAA is used as a template for fabricating the polymer nanostructured gold-capped substrates. This same process is followed for the LSPR immunodetection of cell interleukin-6 from immune cells in real samples[185] and human immunoglobulins.[186,187]

Kim et al. developed a very similar detection system but using aptamers for performing the label-free monitoring of DNA–protein interactions, DNA–DNA hybridizations, and ligand–receptor interactions.[182] A sandwich-type binding assay between two different aptamers and thrombin is reported with an estimated limit of detection of 1×10^{-9} M (**Figure 14**b).[182] This same research group had previously developed this optical system for the detection of synthetic target DNA detection with a 10×10^{-12} M detection limit[188] and also for the detection of CRP protein using in this case an antibody instead of an aptamer.[189]

The higher efficiency inmuno and oligonucleotide-based sensors using LSPR technique are built on NAA substrates with pore diameters of approximately 60 nm. [181,182,186,188,189]

4. NAA Biosensors Detection Targets

4.1. Immunosensors Detection Targets

Several types of targets have been object of study of the health care immunosensors. **Table 1** summarizes all the targets and detection methods explained in this section.

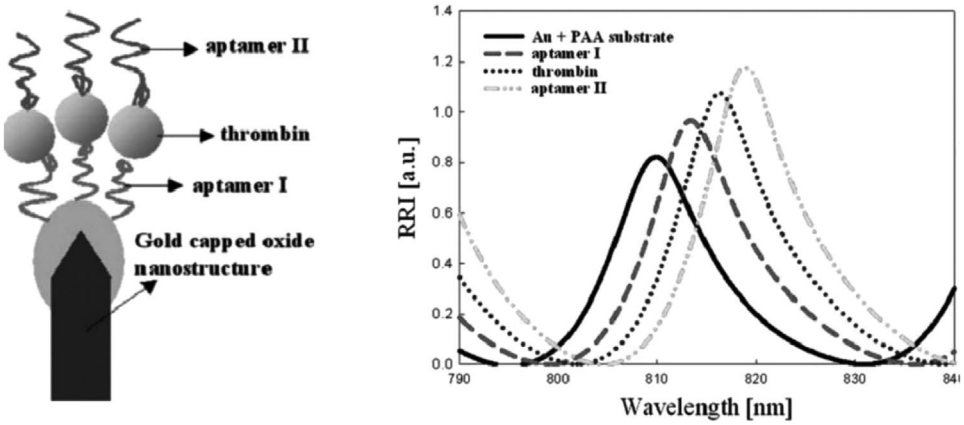

Figure 14. LSPR-based aptasensor for the detection of thrombin. Adapted with permission.[182] Copyright 2008, Elsevier.

Table 1. Target analytes for immunosensors.

	Target analyte	Detection method	Pore diameter	LOD	Medium	Refs.
Virus	Dengue	Impedimetric	Conical from 10–30 to 70–120 nm	1 pfu mL^{-1}	PBS	[122]
	Dengue	Voltammetric	50–100 nm	1 pfu mL^{-1}	PBS	[102]
	West Nile virus	Voltammetry	70 nm	4 pg mL^{-1}	Blood serum	[103]
Bacteria	*Salmonella*	Impedimetric	200 nm	–	PBS	[120]
	E. coli	Impedimetric	60 nm	10 *E. coli* cells/0.173 cm^2 area	PBS	[116]
			100 nm	10 cfu mL^{-1} 83.7 cfu mL^{-1}	PBS whole milk	[117]
			20 nm	10 cfu mL^{-1}	PBS	[119]
	E. coli	Voltammetric	–	22 cfu mL^{-1}	PBS	[101]
	Staphylococcus aureus and *E. coli*	Impedimetric	100 nm	100 cfu mL^{-1}	PBS	[118]
	Bacterial hyaluronidases (HYAL)	Voltammetric	20 nm	64 UI mL^{-1} (17.3 U mg^{-1})	PBS and culture	[100]
Cancer biomarkers	Galectin proteins	Fluorescence	–	160 ng mL^{-1}	*E. coli*-spiked cell lysates	[136]
	Exosomes	LSPR	100 nm	1 ng mL^{-1}	PBS	[183]
	Exosomes	Voltammetric	25 nm	7.3×10^3 particles mL^{-1}	PBS and plasma	[104]
	CA15-3	Voltammetry	200 nm	52 U mL^{-1}	Blood	[112]
	Tumor cells	RIfS	32 ± 3 nm	<1000 cells mL^{-1} 10 000 cells mL^{-1}	PBS blood	[163]
Tumor necrosis biomarker	TNF-α	RIfS	55 ± 3 nm	0.13 µg mL^{-1} 1.5 µg mL^{-1}	PBS simulated wound fluid	[162]
Humoral and cellular inflammatory biomarker	C-reactive protein	LSPR	50 nm 60 nm	1 fg mL^{-1} 1 pg mL^{-1}	Tris–HCl PBS	[181] [189]
Inflammatory biomarker	Interleukin-6	LSPR	120 nm	10 ng mL^{-1}	–	[185]
Inflammatory and cardiovascular biomarker	C-reactive protein (CRP) and myeloperoxidase (MPO)	Impedimetric	40 nm	1 pg mL^{-1}	Isotonic buffer and human serum	[121]
Immune system biomarker	Immunoglobulin	LSPR	40–65 nm –	1 ng mL^{-1} 10 ng μL^{-1}	PBS –	[186] [187]
	Immunoglobulins	Fluorescence	200 nm 200 nm	0.02 ng mL^{-1} 0.1 mg mL^{-1}	Fetal bovine serum PBS	[134] [135]
Wound chronicity biomarker	Flightless I (Flii) protein	Voltammetric	65 nm 200 nm	1.01 µg mL^{-1} 0.5 ng mL^{-1}	In vitro wound model PBS	[113] [114]
Allergen	Histamine	Impedimetric	100 nm	3×10^{-9} M	PBS	[123]

4.1.1. Viruses

Dengue virus, spread out by the mosquito Aedes aegypti, causes the infectious tropical disease dengue fever, which worldwide affects almost 400 million people every year.[190] A rapid and reliable detection of Dengue virus is urgently required to facilitate a fast sanitary response and to prevent epidemics. Dengue virus has been detected using NAA substrate platforms with Anti dengue serotype 2 antibody by voltammetry[102] and impedimetric spectroscopy.[122]

Another virus transmitted by a mosquito is the West Nile virus. The infection caused by this virus can cause in some people inflammation of the spinal cord or brain. In the work of Nguyen et al., this virus is detected using anti-WNV-DIII immunoglobulin M (IgM) as the biorecognition probe with voltametric detection technique.[103]

4.1.2. Bacteria

Escherichia coli is a bacterium commonly found in the lower intestine. Although some strains of *E. coli* can cause mild effects, some others can produce hemolytic uremic syndrome (HUS) resulting in death, especially in children. The detection of this bacterium has been one of the most pursued objectives in the development of immunosensors, being impedimetric spectroscopy the most frequently applied detection method.[116–119] Voltammetric detection has also been used for *E. coli* sensing.[101]

Staphylococcus aureus is also detected by impedimetric sensing.[118] Among the different types of *Staphylococcus*, *Staphylococcus aureus* is the most dangerous of all. Often causes skin infections, but it can cause pneumonia, heart valve infections, and bone infections.

Gram-positive bacteria like *Streptococcus*, *Staphylococcus*, *Streptomyces*, or *Clostridium bacteria* among others use Bacterial hyaluronidases (HYAL) as a virulence factor to destroy the polysaccharide that holds human cells together, and facilitate the pathogens to spread through the body tissues.[191] The quantification of this bioelement therefore has attracted the interest of Escosura-Muniz et al. for the development of a voltammetric biosensor.[100]

4.1.3. Biomarkers

Among the many biomarkers detected in the development of biosensors, cancer biomarkers are the most studied due to their great impact on the health of the world population. Cancer is the second leading cause of death in the world. It causes 10 million deaths every year. Approximately one out of six deaths in the world is due to this disease. Galectins are excellent targets for tumor diagnostics and medical prognostic purposes. Several types of galectins are detected by fluorescence in ref. [136] with a LOD of 4 ng in *E. coli*-spiked cell lysates. Exosomes, membrane-bound extracellular vesicles present in biological fluids constitute novel biomarkers for the monitoring and prediction of cancer diseases. Voltammetry and LSPR are the detection methods used in refs. [104] and [183], respectively, for their successful detection. Cancer biomarker CA15-3 spiked in blood samples is detected by voltammetry.[112] CA15-3 is a glycoprotein mainly used to study patients with breast cancer. RIfS has been the detection method for the biorecognition of circulating tumor cells, concretely pancreatic cancer cells, with the use of anti-EpCAM antibody.[163]

Biomarkers for other diseases have also been detection target of biosensors. Tumor necrosis factor-alpha (TNF-α) is a proinflammatory cytokine important to wound healing. Rajeev et al. used RIfS method for its detection.[162] C-reactive protein (CRP) is a humoral and inflammatory biomarker whose concentration in serum increases dramatically during infections or tissue damage. Impedimmetric detection[121] and LSPR[181,189] have been the two methods used for the development of immunosensors. Other inflammatory proteins like myeloperoxidase—important for identifying patient risk to cardiovascular disease -, and interleukin-6 protein—marker of immune system activation, autoimmune disorders, and cardiovascular diseases—have been quantified using impedimmetry[121] and LSPR,[185] respectively. Immunoglobulins are immune systems biomarkers, they are part of the adaptive immune response, in what is known as a specific humoral response. They constitute a highly effective defense against pathogens, by recognizing and binding to particular antigens, and by helping in their destruction. They have been detected using LSPR[186,187] and fluorescence[134,135] techniques. Wound chronicity biomarker Flightless I, a negative regulator of wound healing present at high level in chronic, nonhealing wounds is detected by voltammetry.[113,114]

4.1.4. Allergens

Histamine can produce allergic reactions such as hypotension, flushing, diarrhea, vomiting, and headaches. Although the symptoms may be different depending on every person, high levels of histamine can cause sneeze, tear up, or itch. Impedimmetry is the detection method used in ref. [123] for its monitoring.

4.2. Oligonucleotide-Based Detection Targets

Several types of targets have been object of study of the health care oligonucleotide-based sensors. **Table 2** summarizes all the targets and detection methods explained in this section.

4.2.1. Viruses

Dengue virus (already explained in Section 5.1.) has been detected by impedimetric sensing in the works of Deng and Toh[130] and Rai et al.[131]

Ebola virus disease, formerly called Ebola hemorrhagic fever, is a serious and very often mortal disease in humans. This virus is transmitted to humans by wild animals and spreads in human populations by person-to-person transmission. Ebola virus disease outbreaks have a fatality rate of approximately 50%. A biosensor for the monitoring of this virus has been developed using fluorescence detection.[139]

4.2.2. Bacteria

Escherichia coli and *Staphylococcus aureus* are two types of bacteria detected using both aptamers and antibodies as biorecognition elements. *E. coli* has been detected by impedimetric spectroscopy[124] and an ultrasensitive biosensor has been developed with molecular gates for *Staphylococcus aureus*.[150]

Salmonella, *listeria*, and *legionella* are bacteria that generally enter the body through food routes seriously affecting human health, even with moral consequences. Current detection methods require long time-consuming processes that delay the medical prognosis and therefore the beginning of medication, causing deterioration of health. Oligonucleotide-based sensors are a rapid and reliable alternative to current diagnosis methods. *Salmonella* is detected by RIfS,[167] legionella is detected by impedimetric spectroscopy,[132] and voltammetry is used for listeria monitoring.[105]

Mycoplasma is a bacteria immune to common antibiotics and related to important pathologies such as pneumonia, rheumatoid arthritis, cancer, and non-gonococcal urogenital diseases, among others. A molecular gate-based system is developed by Pla et al. for its aptamer-based detection.[143]

4.2.3. Fungus

The genus *Candida* comprises a series of phenotypically similar but genetically distant yeasts that produce fungal infections of varying degrees of severity. *Candida albicans* is the most common invasive fungal disease, that in extreme cases can cause peritonitis and intraabdominal abscesses. *Candida auris* is an emerging multidrug-resistant yeast that causes

Table 2. Target analytes for oligonucleotide-based sensors.

	Target analyte	Detection method	Pore diameter	LOD	Medium	Refs.
Virus	Ebola	Fluorescence	–	7×10^{-12} M	Human serum	[139]
	Dengue	Impedimetric	20, 200 nm	2.7×10^{-12} M	Tris buffer	[130]
			–	9.55×10^{-12} M	Tris buffer	[131]
Bacteria	*Salmonella*	RIfS	50 nm	0.01×10^{-9}M	PBS	[167]
	Listeria monocytogenes	Voltammetry	20 nm	100 CFU mL^{-1}	KCl	[105]
	Legionella	Impedimetric	10–150 nm	0.31×10^{-12}M	Tris buffer	[132]
	E. coli	Impedimetric	100 nm	11×10^{-12} M	–	[124]
	Staphylococcus aureus	Molecular gate	5 nm	2 CFU mL^{-1} 5 CFU mL^{-1}	PBS blood	[150]
	Mycoplasma	Molecular gate	8 nm	20 DNA copies mL^{-1}	Tris buffer	[143]
Fungus	*Pneumocystis jirovecii*	Molecular gate	5 nm	1 nm	Tris hybridization buffer, bronchoalveolar lavage, nasopharyngeal aspirates, and sputum	[151]
	Candida albicans	Molecular gate	5 nm	6 CFU mL^{-1}	Tris hybridization buffer and human serum	[142]
	Candida Auris	Molecular gate	7.5 nm	8 CFU mL^{-1}	Tris hybridization buffer and cerebrospinal fluid	[141]
Cancer biomarkers	Circulating microRNA miR-99-5p	Molecular gate	5 nm	0.5×10^{-9} M	Tris hybridization buffer and human plasma	[153]
	8-oxo-7,8-dihydro-2'-deoxyguanosine	Molecular gate	5 nm	1×10^{-9} M 50×10^{-9} M 1×10^{-9} M	Tris hybridization buffer urine human serum	[152]
	RAK I	Fluorescence	150 nm	–	Water and blood	[138]
	miR-21	Voltammetry	200 nm	31×10^{-18} M	PBS and human serum	[108]
	Mucin1	Voltammetry	≈30 nm	0.0364 fg mL^{-1}	KCl	[98]
Coagulation and cancer biomarker	Thrombin	LSPR	60 nm	1×10^{-9} M	PBS	[182]
	Thrombin	Impedimetric	20 nm	10×10^{-12} M	PBS	[129]
	Thrombin	Voltammetry	50 nm	1×10^{-12} M	PBS	[99]
			200 nm	1 nm mL^{-1} 1.8 ng mL^{-1}	PBS Blood	[111]
	Thrombin	RIfS	60 nm	7.2×10^{-9} M	PBS	[68]
Angiocardiopathy & hypoglycaemia biomarker	Adenosine triphosphate (ATP) and potassium (K)	Voltammetry	25 nm	5×10^{-6} M (ATP) and 0.4×10^{-6} M (K)	Tris buffer	[106]
Neural and brain biomarker	Adenosine monophosphate	Impedimetric	11 nm	10×10^{-9} M	HEPES buffer	[125]
Alzheimer's disease biomarkers	Amyloid β	RIfS	54 nm	0.02 µg mL^{-1}	PBS	[168]
Drug	Cocaine	Molecular gate	8 nm	0.5×10^{-6} M 63×10^{-6} M	Hybridization buffer saliva	[140]
	Theophylline	RIfS	10, 50 nm	0.05×10^{-6} M	PBS	[164]
Allergen	Gliadin (Gluten)	Molecular gate	5 nm	100 µg kg^{-1} 250 µg kg^{-1}	Tris buffer Mijo extracts	[154]
	Salicylic acid	RIfS	–	0.1×10^{-6} M	Buffer	[172]
Toxic	Lead	Voltammetry	20 nm	0.1×10^{-9} M	Tris–HCl	[107]
DNA sensing	DNA	Fluorescence	32 nm	20×10^{-12} M	PBS	[137]
	DNA	RIfS	60 nm	–	–	[165]
			70 nm	–	Tris buffer	[166]
	DNA	LSPR	60 nm	10×10^{-12}M	PBS	[188]
	DNA	Voltammetry	Conical from 20 to 200 nm	1×10^{-12}M	PBS	[110]
	DNA	Impedimetric	–	100×10^{-12} M	Tris buffer	[126]
			120 nm	12.5×10^{-9} M	PBS	[127]
			100 nm	50×10^{-12} M	PBS	[128]

serious invasive infections and high mortality, it is extremely dangerous and its detection and control are challenging to prevent transmission. Both species have been detected with ultrasensitive molecular gate-based sensing platforms developed by the research group of Martínez-Máñez using appropriate aptamers.[141,142] The same sensing system has been also used for the detection of *Pneumocystis jirovecii*,[151] the fungus that produces the *Pneumocystis pneumonia* disease and that can be easily disseminated from person to person producing asymptomatic or severe infections.

4.2.4. Biomarkers

Due to the worldwide importance of cancer, the biomarkers indicating an early detection of any type of this disease have been object of intense research. Circulating microRNAs (miRNAs) have emerged as potential diagnostic biomarkers. miRNAs are a class of RNA that can play important role in cellular processes. Altered levels of certain circulating miRNA have been associated with the early detection of cancer.[192] Concretely, miR-99a-5p and miR-21 have been described as effective biomarkers of early breast cancer. The former is detected and quantified with a molecular gate-based system[153] and the latter with voltammetry.[108] Molecular gate-based sensing platforms are also used for the detection of another oncomarker, 8-oxo-7,8-dihydro-2'-deoxyguanosine (8-oxo-dG).[152] This molecule is a product of oxidative stress processes over nucleophilic bases in DNA. High levels of 8-oxo-dG are indicative of colorectal tumors, digestive tumors, ovarian epithelial carcinoma, prostate cancer, or chronic lymphoblastic leukemia. Fluorescence is the detection technique applied to the detection of RAK I,[138] a biomarker of prostate, breast, and gynecological cancer. Finally, the breast and epithelial cancer biomarker Mucin 1 is sensed with voltammetric techniques.[98]

Thrombin is a biomarker of several diseases. The detection of thrombin in blood is of great importance in clinical analysis. The thrombin–fibrinogen interaction is part of the physiological process of blood clotting and altered levels of thrombin are associated with coagulation abnormalities, thrombosis, and platelet activation. Thrombin is also considered an oncomarker of pulmonary metastasis.[111] The great importance of thrombin in human health is reflected in the number of sensing systems developed for its detection. Voltammetry has been used by Zhao et al.[99] and de la Escosura-Muñiz et al.,[111] impedimetry by Gosai et al.,[129] RIfS by Pol et al.,[68] and LSPR by Kim et al.[182]

Adenosine monophosphate contributes to the formation of adenosine, involved in different neural processes in the brain like sleep, arousal, and locomotion. It is considered an important brain and neural biomarker. Peinetti et al. detect and quantify low levels of adenosine monophosphate by impedimetry.[125] On the other hand, adenosine triphosphate (ATP) is a studied biomarker for other types of diseases. Its abnormal levels are closely related to angiocardiopathy and hypoglycemia.[193] The work of Yu et al.[106] presents a voltammetric sensor for the detection of ATP and potassium, also known for its effect on modifiable chronic diseases like hypertension, cardiac disease, diabetes (type-2), and bone health.[194]

Alzheimer's disease is the most common type of dementia that affects more than 32 million people worldwide according to the World Health Organization. Alzheimer's disease affects parts of the brain that control thought, memory, and language, being aging the best-known risk factor. An early diagnosis is crucial to start treatments and slow down its effects. Tabrizi et al. develop a fluorescence biosensor with enhanced sensitivity for the detection of amyloid β, an Alzheimer's disease biomarker present in blood and cerebrospinal fluid.[168]

4.2.5. Drugs

Cocaine is the most commonly consumed addictive and stimulant drug in the world, obtained from coca plant leaves. Its consumption causes a short-term intense high, immediately followed by intense depression, erratic, violent behavior, and dependence. A rapid and ultrasensitive molecular gate-based biosensor is developed by Ribes et al.[140] for the selective detection of cocaine in saliva.

On the contrary, theophylline is a drug used for the treatment of respiratory diseases such as asthma due to its bronchodilatory effect. However, high concentrations of theophylline in blood are toxic and can be lethal or lead to permanent neurological damage, being important to be quickly and regularly monitored in clinical practice. An ultrafast and sensitive RIfS system for the detection of theophylline is developed by Feng et al.[164]

4.2.6. Allergens and Toxics

Gluten is a protein in wheat, barley, and rye. Millions of people worldwide are affected by digestive and health problems caused by consuming gluten. One of the more serious causes of a reaction to gluten is celiac disease, an autoimmune disease affecting almost 1% of world population. A rapid (less than 60 min) and selective detector of gliadin (gluten's soluble proteins) is developed by Pla et al. using molecular gates.[154]

Salicylates have potential disease-preventive activity; however, they can cause health problems to hypersensitive people. Salicylic acid is one of these salicylates most commonly used in clinical practice. Its current detection methods are costly, labor-intensive, and require bulky instruments. Wang et al. develop a cost-effective, rapid, sensitive and simple salicylic acid detection system based on RIfS.[172]

Lead levels in blood are important for the detection of lead poisoning. Voltammetry is the detection method used by Chen et al. for the fast and sensitive detection of lead ions.[107]

4.2.7. DNA Sensing

The development of DNA sensors is of significant medical importance, as they are of great importance in infectious disease diagnosis.[195] For example, in viral infections, the genetic material of the virus inside an infected host can be detected using a complementary capture probe. The development of fast biosensors for cancerous mutation detection is also

medically important. DNA sensors have been developed with NAA oligonucleotide modified substrates using several detection techniques: voltammetry,[110] impedimetric sensing,[126–128] RIfS,[165,166] fluorescence,[137] and LSPR.[188]

5. Conclusions and Future Perspective

In this review, we have summarized the recent progress and key findings in the development of NAA-based sensing systems for the monitoring of health bioelements. NAA has demonstrated to be a decisive platform for optical and electrochemical biosensors allowing the development of fast, label-free ultrasensing and selective devices. Especially important is the use of these biosensors for the detection of biomarkers, allowing an early diagnosis of great incidence diseases like cancer. We have discussed the different types and mechanisms of biosensors based on antibody and oligonucleotide receptors, classified for their detection method (voltammetry, impedance spectroscopy, fluorescence, RIfS, and LSPR). The initial success of immunosensors for the detection of several analytes was followed by the appearance of synthesized nucleic acid sequences (generally called aptamers), more stable and specific than antibodies and produced by a simple, inexpensive, and time reduced process. The arrival of aptamers has revolutionized and revitalized the development of biosensors with increased sensitivity (≈1 fg mL^{-1}) and selectivity.

Now and in the next years, antibody and oligonucleotide-based biosensors will continue offering versatile and point-of care systems for the detection of viruses, bacteria, allergens, toxics, drugs, and several disease biomarkers, including many types of cancer. The results and the technology presented in this review demonstrate the important advantages and versatility of NAA biosensors for developing commercial elements and devices for industrial application. Some of the presented biosensors (molecular gate sensors), with excellent detection properties and low production cost, have been worldwide patented and have current clinical applications. The maturity level and outputs of others demonstrate their utility and potential for real mankind healthcare. The great current pandemic that humanity is currently facing has arisen the immediate necessity of sensors with fast, reliable, and highly sensitivity detection of the virus incubation in patients. And not only for the virus expanded nowadays but also for other new viruses in a near or far future that is predicted to appear. In this line, NAA immune and oligonucleotide-based sensing platforms, with their high versatility and adaptability are real. feasible, and useful systems to be used for this purpose, being able to identify and quantify with the presented techniques any biological target with the adequate NAA surface functionalization. The main current challenges to be addressed are the development of alternative functionalization processes, the finding of new disease biomarkers, and the development of high-affinity aptamers for specific bioagents recognition. The improvement and evolution of all these aspects will lead to excellent NAA biosensors, essential sensing and quantification elements for any type of disease, and with decisive use for clinical and point-of-care diagnosis and theragnostics.

Acknowledgements

This work was further supported by the Spanish Ministerio de Ciencia, Innovación y Universidades (MICINN/FEDER) RTI2018-094040-B-I00, by AGAUR ref. 2017-SGR-1527.

Conflict of Interest

The authors declare no conflict of interest.

Keywords

antibodies, aptamers, biosensors, health, immunosensors, nanoporous anodic alumina, oligonucleotides

Received: November 30, 2021
Revised: February 7, 2022
Published online:

[1] S. Ramanavicius, A. Ramanavicius, *Polymers* **2021**, *13*, 49.
[2] S. Ramanavicius, A. Jagminas, A. Ramanavicius, *Polymers* **2021**, *13*, 974.
[3] M. Drobysh, A. Ramanaviciene, R. Viter, A. Ramanavicius, *Micromachines* **2021**, *12*, 390.
[4] J. Dronina, U. Samukaite, A. Ramanavicius, *Biosens. Bioelectron.* **2021**, *175*, 112867.
[5] J. Dronina, U. Samukaite-Bubniene, A. Ramanavicius, *J. Nanobiotechnol.* **2021**, *19*, 348.
[6] M. Drobysh, A. Ramanaviciene, R. Viter, C. F. Chen, U. Samukaite-Bubniene, V. Ratautaite, A. Ramanavicius, *Int. J. Mol. Sci.* **2022**, *23*, 666.
[7] T. Bertok, L. Lorencova, E. Chocholova, E. Jane, A. Vikartovska, P. Kasak, J. Tkac, *ChemElectroChem* **2019**, *6*, 989.
[8] S. A. Lim, M. U. Ahmed, *RSC Adv.* **2016**, *6*, 24995.
[9] A. de la Escosura-Muñiz, A. Merkoçi, *TrAC, Trends Anal. Chem.* **2016**, *79*, 134.
[10] J. Leva-Bueno, S. A. Peyman, P. A. Millner, *Med. Microbiol. Immunol.* **2020**, *209*, 343.
[11] M. A. Tabrizi, J. Ferre-Borrull, L. F. Marsal, *Sensors* **2020**, *20*, 5068.
[12] S. K. Bhardwaj, H. Singh, M. Khatri, K. H. Kim, N. Bhardwaj, *Biosens. Bioelectron.* **2022**, *202*, 113995.
[13] B. Kaur, S. Kumar, B. K. Kaushik, *Biosens. Bioelectron.* **2022**, *197*, 113805.
[14] K. Girigoswami, N. Akhtar, *Int. J. Nano Dimens.* **2019**, *10*, 1.
[15] E. Benito-Peña, M. G. Valdés, B. Glahn-Martínez, M. C. Moreno-Bondi, *Anal. Chim. Acta* **2016**, *943*, 17.
[16] Y. Jeong, Y. M. Kook, K. Lee, W. G. Koh, *Biosens. Bioelectron.* **2018**, *111*, 102.
[17] J. P. O'sullivan, G. C. Wood, *Proc. R. Soc. London, Ser. A* **1970**, *317*, 511.
[18] G. E. Thompson, G. C. Wood, *Nature* **1981**, *290*, 230.
[19] G. D. Sulka, in *Nanostructured Materials in Electrochemistry*, (Ed: A. Eftekhari), Wiley-VCH, Weinheim, Germany **2008**, pp. 1–116.
[20] S. Ono, M. Saito, H. Asoh, *Electrochim. Acta* **2005**, *51*, 827.
[21] A. M. Md Jani, D. Losic, N. H. Voelcker, *Prog. Mater. Sci.* **2013**, *58*, 636.
[22] A. Eftekhari, in *Nanostructured Materials in Electrochemistry* (Ed: A. Eftekhari), Wiley-VCH, Weinheim, Germany **2008**, pp. 1–463.
[23] W. Lee, K. Schwirn, M. Steinhart, E. Pippel, R. Scholz, U. Gösele, *Nat. Nanotechnol.* **2008**, *3*, 234.

[24] W. Lee, S.-J. Park, *Chem. Rev.* **2014**, *114*, 7487.
[25] H. Han, S. J. Park, J. S. Jang, H. Ryu, K. J. Kim, S. Baik, W. Lee, *ACS Appl. Mater. Interfaces* **2013**, *5*, 3441.
[26] M. M. Rahman, E. Garcia-Caurel, A. Santos, L. F. Marsal, J. Pallarès, J. Ferré-Borrull, *Nanoscale Res. Lett.* **2012**, *7*, 474.
[27] H. Masuda, K. Fukuda, *Science* **1995**, *268*, 1466.
[28] O. Jessensky, F. Müller, U. Gösele, *Appl. Phys. Lett.* **1998**, *72*, 1173.
[29] K. Nielsch, J. Choi, K. Schwirn, R. B. Wehrspohn, U. Gösele, *Nano Lett.* **2002**, *2*, 677.
[30] H. Masuda, H. Yamada, M. Satoh, H. Asoh, M. Nakao, T. Tamamura, *Appl. Phys. Lett.* **1997**, *71*, 2770.
[31] D. Wang, L. Zhang, W. Lee, M. Knez, L. Liu, *Small* **2013**, *9*, 1025.
[32] I. Mikulskas, S. Juodkazis, R. Tomasiūnas, J. G. Dumas, *Adv. Mater.* **2001**, *13*, 1574.
[33] G. Meng, Y. J. Jung, A. Cao, R. Vajtai, P. M. Ajayan, *Proc. Natl. Acad. Sci. USA* **2005**, *102*, 7074.
[34] W. Cheng, M. Steinhart, U. Gösele, R. B. Wehrspohn, *J. Mater. Chem.* **2007**, *17*, 3493.
[35] K. Nielsch, F. Müller, A.-P. Li, U. Gösele, *Adv. Mater.* **2000**, *12*, 582.
[36] A. Santos, L. Vojkuvka, J. Pallarés, J. Ferré-Borrull, L. F. Marsal, *Nanoscale Res. Lett.* **2009**, *4*, 1021.
[37] A. Santos, P. Formentin, J. Pallarés, J. Ferré-Borrull, L. F. Marsal, *Mater. Lett.* **2010**, *64*, 371.
[38] W. Lee, R. Scholz, U. Gösele, *Nano Lett.* **2008**, *8*, 2155.
[39] W. J. Zheng, G. T. Fei, B. Wang, Z. Jin, L. De Zhang, *Mater. Lett.* **2009**, *63*, 706.
[40] W. Zheng, G. Fei, B. Wang, L. De Zhang, *Nanoscale Res. Lett.* **2009**, *4*, 665.
[41] J. Ferré-Borrull, M. M. Rahman, J. Pallarès, L. F. Marsal, *Nanoscale Res. Lett.* **2014**, *9*, 416.
[42] A. Santos, M. Alba, M. M. Rahman, P. Formentín, J. Ferré-Borrull, J. Pallarès, L. F. Marsal, *Nanoscale Res. Lett.* **2012**, *7*, 228.
[43] G. Macias, J. Ferré-Borrull, J. Pallarès, L. F. Marsal, *Nanoscale Res. Lett.* **2014**, *9*, 315.
[44] T. Kumeria, A. Santos, M. M. Rahman, J. Ferré-Borrull, L. F. Marsal, D. Losic, *ACS Photonics* **2014**, *1*, 1298.
[45] L. K. Acosta, F. Berto-Rosello, E. Xifre-Perez, A. Santos, J. Ferre-Borull, L. F. Marsal, *ACS Appl. Mater. Interfaces* **2019**, *11*, 3360.
[46] A. Santos, V. S. Balderrama, M. Alba, P. Formentín, J. Ferré-Borrull, J. Pallarès, L. F. Marsal, *Nanoscale Res. Lett.* **2012**, *7*, 370.
[47] J. Li, C. Li, C. Chen, Q. Hao, Z. Wang, J. Zhu, X. Gao, *ACS Appl. Mater. Interfaces* **2012**, *4*, 5678.
[48] A. Santos, P. Formentín, J. Pallarès, J. Ferré-Borrull, L. F. Marsal, *J. Electroanal. Chem.* **2011**, *655*, 73.
[49] T. Nagaura, F. Takeuchi, S. Inoue, *Electrochim. Acta* **2008**, *53*, 2109.
[50] A. Santos, T. Kumeria, Y. Wang, D. Losic, *Nanoscale* **2014**, *6*, 9991.
[51] M. Porta-i-Batalla, E. Xifré-Pérez, C. Eckstein, J. Ferré-Borrull, L. F. Marsal, *Nanomaterials* **2017**, *7*, 227.
[52] A. Santos, L. Vojkuvka, M. Alba, V. S. Balderrama, J. Ferré-Borrull, J. Pallarès, L. F. Marsal, *Phys. Status Solidi A* **2012**, *209*, 2045.
[53] A. Santos, J. Ferré-Borrull, J. Pallarès, L. F. Marsal, *Phys. Status Solidi A* **2011**, *208*, 668.
[54] V. Szczepanski, I. Vlassiouk, S. Smirnov, *J. Membr. Sci.* **2006**, *281*, 587.
[55] C. Eckstein, C. S. Law, S. Y. Lim, S. Kaur, T. Kumeria, J. Ferré-Borrull, A. D. Abell, L. F. Marsal, A. Santos, *J. Mater. Chem. C* **2019**, *7*, 12278.
[56] C. Eckstein, L. K. Acosta, L. Pol, E. Xifré-Pérez, J. Pallares, J. Ferré-Borrull, L. F. Marsal, *ACS Appl. Mater. Interfaces* **2018**, *10*, 10571.
[57] L. Pol, C. Eckstein, L. K. Acosta, E. Xifré-Pérez, J. Ferré-Borrull, L. F. Marsal, *Nanomaterials* **2019**, *9*, 478.
[58] T. D. Lazzara, T. T. Kliesch, A. Janshoff, C. Steinem, *ACS Appl. Mater. Interfaces* **2011**, *3*, 1068.
[59] T. D. Lazzara, K. H. A. Lau, A. I. Abou-Kandil, A. M. Caminade, J. P. Majoral, W. Knoll, *ACS Nano* **2010**, *4*, 3909.
[60] C. Eckstein, E. Xifré-Pérez, M. Porta-i-Batalla, J. Ferré-Borrull, L. F. Marsal, *Langmuir* **2016**, *32*, 10467.
[61] M. Porta-i-Batalla, C. Eckstein, E. Xifré-Pérez, P. Formentín, J. Ferré-Borrull, L. F. Marsal, *Nanoscale Res. Lett.* **2016**, *11*, 372.
[62] P. Kapruwan, L. K. Acosta, J. Ferré-Borrull, L. F. Marsal, *Nanomaterials* **2021**, *11*, 730.
[63] D. M. Dotzauer, J. H. Dai, L. Sun, M. L. Bruening, *Nano Lett.* **2006**, *6*, 2268.
[64] I. Minguez-Bacho, S. Rodriguez-López, M. Vázquez, M. Hernández-Vélez, K. Nielsch, *Nanotechnology* **2014**, *25*, 145301.
[65] A. Jagminas, J. Kuzmarskytė, G. Valinčius, L. Malferrari, A. Malinauskas, *Nanoscale Res. Lett.* **2007**, *2*, 130.
[66] A. Johansson, J. Lu, J. O. Carlsson, M. Boman, *J. Appl. Phys.* **2004**, *96*, 5189.
[67] S. Z. Chu, H. Kawamura, M. Mori, *J. Electrochem. Soc.* **2008**, *155*, D414.
[68] L. Pol, L. K. Acosta, J. Ferré-Borrull, L. F. Marsal, *Sensors* **2019**, *19*, 4543.
[69] L. P. Hernández-Eguía, J. Ferré-Borrull, G. Macias, J. Pallarès, L. F. Marsal, *Nanoscale Res. Lett.* **2014**, *9*, 414.
[70] T. R. B. Foong, Y. Shen, X. Hu, A. Sellinger, *Adv. Funct. Mater.* **2010**, *20*, 1390.
[71] L. Y. Wen, Y. Mi, C. L. Wang, Y. G. Fang, F. Grote, H. P. Zhao, M. Zhou, Y. Lei, *Small* **2014**, *10*, 3162.
[72] T. Altalhi, M. Ginic-Markovic, N. Han, S. Clarke, D. Losic, *Membranes* **2010**, *1*, 37.
[73] M. Alsawat, T. Altalhi, T. Kumeria, A. Santos, D. Losic, *Carbon* **2015**, *93*, 681.
[74] W. Y. Jang, N. N. Kulkarni, C. K. Shih, Z. Yao, *Appl. Phys. Lett.* **2004**, *84*, 1177.
[75] M. Sarno, A. Tamburrano, L. Arurault, S. Fontorbes, R. Pantani, L. Datas, P. Ciambelli, M. S. Sarto, *Carbon* **2013**, *55*, 10.
[76] H. W. Schroeder, L. Cavacini, *J. Allergy Clin. Immunol.* **2010**, *125*, S41.
[77] C. J. van Oss, R. J. Good, M. K. Chaudhury, *J. Chromatogr. B: Biomed. Sci. Appl.* **1986**, *376*, 111.
[78] I. Sela-Culang, V. Kunik, Y. Ofran, *Front. Immunol.* **2013**, *4*, 302.
[79] E. B. Aydin, M. Aydin, M. K. Sezgintürk, *Adv. Clin. Chem.* **2019**, *92*, 1.
[80] K. Mahato, S. Kumar, A. Srivastava, P. K. Maurya, R. Singh, P. Chandra, in *Handbook of Immunoassay Technologies: Approaches, Performances, and Applications*, (Eds: S. Vashist, J. Luong), Elsevier, Amsterdam **2018**, pp. 359–414.
[81] T. R. J. Holford, F. Davis, S. P. J. Higson, *Biosens. Bioelectron.* **2012**, *34*, 12.
[82] H. Bhardwaj, G. Sumana, C. A. Marquette, *Talanta* **2021**, *222*, 121578.
[83] A. C. H. de Castro, L. M. Alves, A. C. S. Siquieroli, J. M. Madurro, A. G. Brito-Madurro, *Microchem. J.* **2020**, *155*, 104746.
[84] T. C. Roberts, R. Langer, M. J. A. Wood, *Nat. Rev. Drug Discovery* **2020**, *19*, 673.
[85] J. Carvalho, J. Lopes-Nunes, A. C. Lopes, M. P. Cabral Campello, A. Paulo, J. A. Queiroz, C. Cruz, *Org. Biomol. Chem.* **2019**, *17*, 2992.
[86] N. Saraf, M. Villegas, B. J. Willenberg, S. Seal, *ACS Omega* **2019**, *4*, 2234.
[87] Y. Chen, W. Wang, D. Tyagi, A. J. Carrier, S. Cui, S. He, X. Zhang, *Nanoscale* **2019**, *11*, 5879.
[88] H. Chai, X. Ma, F. Meng, Q. Mei, Y. Tang, P. Miao, *New J. Chem.* **2019**, *43*, 7928.
[89] W. Hou, Y. Liu, Y. Jiang, Y. Wu, C. Cui, Y. Wang, L. Zhang, I. T. Teng, W. Tan, *Nanoscale* **2018**, *10*, 10986.
[90] N. Patel, S. Patel, *J. Nanomed. Res.* **2017**, *5*, 134.
[91] G. Zhu, G. Niu, X. Chen, *Bioconjugate Chem.* **2015**, *26*, 2186.
[92] C. Chen, S. Zhou, Y. Cai, F. Tang, *npj Precis. Oncol.* **2017**, *1*, 37.
[93] M. McKeague, M. C. DeRosa, *J. Nucleic Acids* **2012**, *2012*, 748913.

[94] M. McKeague, E. M. McConnell, J. Cruz-Toledo, E. D. Bernard, A. Pach, E. Mastronardi, X. Zhang, M. Beking, T. Francis, A. Giamberardino, A. Cabecinha, A. Ruscito, R. Aranda-Rodriguez, M. Dumontier, M. C. DeRosa, *J. Mol. Evol.* **2015**, *81*, 150.
[95] Q. Yan, M. Cai, L. Zhou, H. Xu, Y. Shi, J. Sun, J. Jiang, J. Gao, H. Wang, *Nanoscale Adv.* **2019**, *1*, 291.
[96] R. Stoltenburg, C. Reinemann, B. Strehlitz, *Biomol. Eng.* **2007**, *24*, 381.
[97] V. Thiviyanathan, D. G. Gorenstein, *Proteomics: Clin. Appl.* **2012**, *6*, 563.
[98] M. Pan, J. Cai, S. Li, L. Xu, W. Ma, C. Xu, H. Kuang, *Anal. Chem.* **2021**, *93*, 4825.
[99] X. P. Zhao, J. Cao, X. G. Nie, S. S. Wang, C. Wang, X. H. Xia, *Electrochem. Commun.* **2017**, *81*, 5.
[100] A. D. La Escosura-Muniz, K. Ivanova, T. Tzanov, *ACS Appl. Mater. Interfaces* **2019**, *11*, 13140.
[101] M. S. Cheng, S. H. Lau, V. T. Chow, C. S. Toh, *Environ. Sci. Technol.* **2011**, *45*, 6453.
[102] M. S. Cheng, J. S. Ho, C. H. Tan, J. P. S. Wong, L. C. Ng, C. S. Toh, *Anal. Chim. Acta* **2012**, *725*, 74.
[103] B. T. T. Nguyen, G. Koh, H. S. Lim, A. J. S. Chua, M. M. L. Ng, C.-S. Toh, *Anal. Chem.* **2009**, *81*, 7226.
[104] C. Wang, D. Jin, Y. Yu, L. Tang, Y. Sun, Z. Sun, G. J. Zhang, *Sens. Actuators, B* **2020**, *314*, 128056.
[105] C. X. Zhou, R. J. Mo, Z. M. Chen, J. Wang, G. Z. Shen, Y. P. Li, Q. G. Quan, Y. Liu, C. Y. Li, *ACS Sens.* **2016**, *1*, 965.
[106] J. Yu, L. Zhang, X. Xu, S. Liu, *Anal. Chem.* **2014**, *86*, 10741.
[107] Z. M. Chen, G. Z. Shen, Y. P. Li, P. Zhang, H. W. Ji, S. C. Liu, C. Y. Li, Z. J. Qian, *Electrochem. Commun.* **2015**, *60*, 83.
[108] Z. Jiang, J. Jiao, J. Li, H. Zhang, J. Zheng, *Sens. Actuators, B* **2021**, *344*, 130209.
[109] S. Ullah, P. John, A. Bhatti, *Mol. Biol. Rep.* **2014**, *41*, 225.
[110] S.-J. Li, N. Xia, B.-Q. Yuan, W.-M. Du, Z.-F. Sun, B.-B. Zhou, *Electrochim. Acta* **2015**, *159*, 234.
[111] A. de la Escosura-Muñiz, W. Chunglok, W. Surareungchai, A. Merkoçi, *Biosens. Bioelectron.* **2013**, *40*, 24.
[112] A. de la Escosura-Muñiz, A. Merkoçi, *Small* **2011**, *7*, 675.
[113] G. Rajeev, E. Melville, A. J. Cowin, B. Prieto-Simon, N. H. Voelcker, *Front. Chem.* **2020**, *8*, 155.
[114] G. Rajeev, A. J. Cowin, N. H. Voelcker, B. P. Simon, *Front. Chem.* **2019**, *7*, 438.
[115] F. Ciucci, *Curr. Opin. Electrochem.* **2019**, *13*, 132.
[116] M. Basu, S. Seggerson, J. Henshaw, J. Jiang, R. D. A. Cordona, C. Lefave, P. J. Boyle, A. Miller, M. Pugia, S. Basu, *Glycoconjugate J.* **2004**, *21*, 487.
[117] C.-K. Joung, H.-N. Kim, M.-C. Lim, T.-J. Jeon, H.-Y. Kim, Y.-R. Kim, *Biosens. Bioelectron.* **2013**, *44*, 210.
[118] F. Tan, P. H. M. Leung, Z. Bin Liu, Y. Zhang, L. Xiao, W. Ye, X. Zhang, L. Yi, M. Yang, *Sens. Actuators, B* **2011**, *159*, 328.
[119] K. Y. Chan, W. W. Ye, Y. Zhang, L. D. Xiao, P. H. M. Leung, Y. Li, M. Yang, *Biosens. Bioelectron.* **2013**, *41*, 532.
[120] W. Ye, J. Guo, X. Bao, T. Chen, W. Weng, S. Chen, M. Yang, *Materials* **2017**, *10*, 603.
[121] K. Lin, V. Kunduru, M. Bothara, K. Rege, S. Prasad, B. L. Ramakrishna, *Biosens. Bioelectron.* **2010**, *25*, 2336.
[122] B. T. T. Nguyen, A. E. K. Peh, C. Y. L. Chee, K. Fink, V. T. K. Chow, M. M. L. Ng, C. S. Toh, *Bioelectrochemistry* **2012**, *88*, 15.
[123] W. Ye, Y. Xu, L. Zheng, Y. Zhang, M. Yang, P. Sun, *Sensors* **2016**, *16*, 1767.
[124] W. Ye, T. Chen, Y. Mao, F. Tian, P. Sun, M. Yang, *Microchim. Acta* **2017**, *184*, 4835.
[125] A. S. Peinetti, H. Ceretti, M. Mizrahi, G. A. González, S. A. Ramírez, F. G. Requejo, J. M. Montserrat, F. Battaglini, *Nanoscale* **2015**, *7*, 7763.
[126] A. S. Peinetti, H. Ceretti, M. Mizrahi, G. A. González, S. A. Ramírez, F. G. Requejo, J. M. Montserrat, F. Battaglini, *Bioelectrochemistry* **2018**, *121*, 169.
[127] S. Wu, W. Ye, M. Yang, M. Taghipoor, R. Meissner, J. Brugger, P. Renaud, *Sens. Actuators, B* **2015**, *216*, 105.
[128] W. W. Ye, J. Y. Shi, C. Y. Chan, Y. Zhang, M. Yang, *Sens. Actuators, B* **2014**, *193*, 877.
[129] A. Gosai, B. S. Hau Yeah, M. Nilsen-Hamilton, P. Shrotriya, *Biosens. Bioelectron.* **2019**, *126*, 88.
[130] J. Deng, C. S. Toh, *Sensors* **2013**, *13*, 7774.
[131] V. Rai, H. C. Hapuarachchi, L. C. Ng, S. H. Soh, Y. S. Leo, C. S. Toh, *PLoS One* **2012**, *7*, e42346.
[132] V. Rai, J. Deng, C. S. Toh, *Talanta* **2012**, *98*, 112.
[133] C. Nicolini, M. Singh, R. Spera, L. Felli, *Bioengineered* **2013**, *4*, 332.
[134] J. Dai, G. L. Baker, M. L. Bruening, *Anal. Chem.* **2006**, *78*, 135.
[135] M. Kang, L. Trofin, M. O. Mota, C. R. Martin, *Anal. Chem.* **2005**, *77*, 6243.
[136] H. Van Hattum, N. I. Martin, R. Ruijtenbeek, R. J. Pieters, *Anal. Biochem.* **2013**, *434*, 99.
[137] Y. Fan, K. Hotta, A. Yamaguchi, Y. Ding, Y. He, N. Teramae, S. Sun, H. Ma, *Appl. Phys. Lett.* **2014**, *105*, 031103.
[138] M. Aramesh, O. Shimoni, K. Fox, T. J. Karle, A. Lohrmann, K. Ostrikov, S. Prawer, J. Cervenka, *Nanoscale* **2015**, *7*, 5998.
[139] M. K. Tsang, W. Ye, G. Wang, J. Li, M. Yang, J. Hao, *ACS Nano* **2016**, *10*, 598.
[140] À. Ribes, E. Xifré-Pérez, E. Aznar, F. Sancenón, T. Pardo, L. F. Marsal, R. Martínez-Máñez, *Sci. Rep.* **2016**, *6*, 38649.
[141] L. Pla, S. Santiago-Felipe, M. Á. Tormo-Mas, A. Ruiz-Gaitán, J. Pemán, E. Valentín, F. Sancenón, E. Aznar, R. Martínez-Máñez, *Emerging Microbes Infect.* **2021**, *10*, 407.
[142] À. Ribes, E. Aznar, S. Santiago-Felipe, E. Xifre-Perez, M. Á. Tormo-Mas, J. Pemán, L. F. Marsal, R. Martínez-Máñez, *ACS Sens.* **2019**, *4*, 1291.
[143] L. Pla, E. Xifré-Pérez, À. Ribes, E. Aznar, M. D. Marcos, L. F. Marsal, R. Martínez-Máñez, F. Sancenón, *ChemPlusChem* **2017**, *82*, 337.
[144] C. L. Zhu, C. H. Lu, X. Y. Song, H. H. Yang, X. R. Wang, *J. Am. Chem. Soc.* **2011**, *133*, 1278.
[145] P. Díez, A. Sánchez, M. Gamella, P. Martínez-Ruíz, E. Aznar, C. De La Torre, J. R. Murguía, R. Martínez-Máñez, R. Villalonga, J. M. Pingarrón, *J. Am. Chem. Soc.* **2014**, *136*, 9116.
[146] Y. L. Choi, J. Jaworski, M. L. Seo, S. J. Lee, J. H. Jung, *J. Mater. Chem.* **2011**, *21*, 7882.
[147] F. Sancenõn, L. Pascual, M. Oroval, E. Aznar, R. Martínez-Máñez, *ChemistryOpen* **2015**, *4*, 418.
[148] L. Hou, C. Zhu, X. Wu, G. Chen, D. Tang, *Chem. Commun.* **2014**, *50*, 1441.
[149] Z. Chen, Y. Tan, K. Xu, L. Zhang, B. Qiu, L. Guo, Z. Lin, G. Chen, *Biosens. Bioelectron.* **2016**, *75*, 8.
[150] L. Pla, S. Santiago-Felipe, M. Á. Tormo-Mas, J. Pemán, F. Sancenón, E. Aznar, R. Martínez-Máñez, *Sens. Actuators, B* **2020**, *320*, 128281.
[151] L. Pla, A. Aviñó, R. Eritja, A. Ruiz-Gaitán, J. Pemán, V. Friaza, E. J. Calderón, E. Aznar, R. Martínez-Máñez, S. Santiago-Felipe, *J. Fungi* **2020**, *6*, 292.
[152] L. Pla, F. Sancenón, M. C. Martínez-Bisbal, C. Bañuls, N. Estañ, M. Botello-Marabotto, E. Aznar, G. Sáez, S. Santiago-Felipe, R. Martínez-Máñez, *Nanoscale* **2021**, *13*, 8648.
[153] I. Garrido-Cano, L. Pla, S. Santiago-Felipe, S. Simón, B. Ortega, B. Bermejo, A. Lluch, J. M. Cejalvo, P. Eroles, R. Martínez-Máñez, *ACS Sens.* **2021**, *6*, 1022.
[154] L. Pla, M. C. Martínez-Bisbal, E. Aznar, F. Sancenón, R. Martínez-Máñez, S. Santiago-Felipe, *Anal. Chim. Acta* **2021**, *1147*, 178.
[155] Y. Chen, A. Santos, Y. Wang, T. Kumeria, C. Wang, J. Li, D. Losic, *Nanoscale* **2015**, *7*, 7770.

[156] T. Kumeria, D. Losic, *Nanoscale Res. Lett.* **2012**, *7*, 88.
[157] T. D. Lazzara, I. Mey, C. Steinem, A. Janshoff, *Anal. Chem.* **2011**, *83*, 5624.
[158] M. C. Estevez, M. Alvarez, L. M. Lechuga, *Laser Photonics Rev.* **2012**, *6*, 463.
[159] A. Santos, T. Kumeria, D. Losic, *Anal. Chem.* **2013**, *85*, 7904.
[160] K. A. Kilian, T. Böcking, K. Gaus, M. Gal, J. J. Gooding, *ACS Nano* **2007**, *1*, 355.
[161] T. Kumeria, K. Gulati, A. Santos, D. Losic, *ACS Appl. Mater. Interfaces* **2013**, *5*, 5436.
[162] G. Rajeev, E. Xifre-Perez, B. Prieto Simon, A. J. Cowin, L. F. Marsal, N. H. Voelcker, *Sens. Actuators, B* **2018**, *257*, 116.
[163] T. Kumeria, M. D. Kurkuri, K. R. Diener, L. Parkinson, D. Losic, *Biosens. Bioelectron.* **2012**, *35*, 167.
[164] S. Feng, C. Chen, W. Wang, L. Que, *Biosens. Bioelectron.* **2018**, *105*, 36.
[165] Q. Q. Wu, K. G. Wang, D. Sun, S. Wang, C. Zhang, W. Zhao, *Chin. Phys. Lett.* **2016**, *33*, 088701.
[166] Y. Lu, D. Sun, K. Wang, X. Bai, C. Zhang, W. Zhao, X. Feng, J. Bai, *Optik* **2019**, *192*, 162903.
[167] M. Amouzadeh Tabrizi, J. Ferré-Borrull, L. F. Marsal, *Sens. Actuators, B* **2020**, *304*, 127302.
[168] M. Amouzadeh Tabrizi, J. Ferré-Borrull, L. F. Marsal, *Biosens. Bioelectron.* **2019**, *137*, 279.
[169] A. F. Chambers, A. C. Groom, I. C. MacDonald, *Nat. Rev. Cancer* **2002**, *2*, 563.
[170] J. S. De Bono, H. I. Scher, R. B. Montgomery, C. Parker, M. C. Miller, H. Tissing, G. V. Doyle, L. W. W. M. Terstappen, K. J. Pienta, D. Raghavan, *Clin. Cancer Res.* **2008**, *14*, 6302.
[171] M. L. Kowalski, R. Asero, S. Bavbek, M. Blanca, N. Blanca-Lopez, G. Bochenek, K. Brockow, P. Campo, G. Celik, J. Cernadas, G. Cortellini, E. Gomes, E. Nizankowska-Mogilnicka, A. Romano, A. Szczeklik, S. Testi, M. J. Torres, S. Wöhrl, J. Makowska, *Allergy Eur. J. Allergy Clin. Immunol.* **2013**, *68*, 1219.
[172] C. Chen, S. Feng, M. Zhou, C. Ji, L. Que, W. Wang, *Biosens. Bioelectron.* **2019**, *140*, 111342.
[173] S. Wang, L. Xu, G. Li, P. Chen, K. Xia, X. Zhou, *Plant Sci.* **2002**, *162*, 529.
[174] A. H. Dawson, I. M. Whyte, *Br. J. Clin. Pharmacol.* **1999**, *48*, 278.
[175] M. Amouzadeh Tabrizi, J. Ferré-Borrull, L. F. Marsal, *Sens. Actuators, B* **2020**, *321*, 128314.
[176] M. Amouzadeh Tabrizi, M. Shamsipur, *Biosens. Bioelectron.* **2015**, *69*, 100.
[177] J. N. Chazalviel, F. Ozanam, *Materials* **2010**, *4*, 825.
[178] M. Chen, H. Su, L. Mao, M. Y. Guo, J. Tang, *Microchim. Acta* **2018**, *185*, 51.
[179] J. Cao, T. Sun, K. T. V. Grattan, *Sens. Actuators, B* **2014**, *195*, 332.
[180] J. R. Mejía-Salazar, O. N. Oliveira, *Chem. Rev.* **2018**, *118*, 10617.
[181] S.-H. Yeom, O.-G. Kim, B.-H. Kang, K.-J. Kim, H. Yuan, D.-H. Kwon, H.-R. Kim, S.-W. Kang, *Opt. Express* **2011**, *19*, 22882.
[182] D.-K. Kim, K. Kerman, H. M. Hiep, M. Saito, S. Yamamura, Y. Takamura, Y.-S. Kwon, E. Tamiya, *Anal. Biochem.* **2008**, *379*, 1.
[183] X. Lv, Z. Geng, Y. Su, Z. Fan, S. Wang, W. Fang, H. Chen, *Langmuir* **2019**, *35*, 9816.
[184] M. Wei, T. Yang, X. Chen, Y. Wu, X. Deng, W. He, J. Yang, Z. Wang, *Oncotarget* **2017**, *8*, 42262.
[185] X. Luo, C. Zhu, M. Saito, W. V. Espulgar, X. Dou, Y. Terada, A. Obara, S. Uchiyama, E. Tamiya, *Bull. Chem. Soc. Jpn.* **2020**, *93*, 1121.
[186] M. Saito, A. Kitamura, M. Murahashi, K. Yamanaka, L. Q. Hoa, Y. Yamaguchi, E. Tamiya, *Anal. Chem.* **2012**, *84*, 5494.
[187] R. A. M. Ali, W. V. Espulgar, W. Aoki, S. Jiang, M. Saito, M. Ueda, E. Tamiya, *Jpn. J. Appl. Phys.* **2018**, *57*, 03EC03.
[188] D. K. Kim, K. Kerman, M. Saito, R. R. Sathuluri, T. Endo, S. Yamamura, Y. S. Kwon, E. Tamiya, *Anal. Chem.* **2007**, *79*, 1855.
[189] D. K. Kim, K. Kerman, S. Yamamura, Y. S. Kwon, Y. Takamura, E. Tamiya, *Jpn. J. Appl. Phys.* **2008**, *47*, 1351.
[190] Y. S. Tian, Y. Zhou, T. Takagi, M. Kameoka, N. Kawashita, *Chem. Pharm. Bull.* **2018**, *66*, 191.
[191] C. B. Ibberson, C. L. Jones, S. Singh, M. C. Wise, M. E. Hart, D. V. Zurawski, A. R. Horswill, *Infect. Immun.* **2014**, *82*, 4253.
[192] G. A. Calin, C. M. Croce, *Nat. Rev. Cancer* **2006**, *6*, 857.
[193] F. Qu, J. Li, W. Han, L. Xia, J. You, *Sensors* **2018**, *18*, 2151.
[194] S. Tabbassum, P. Cheng, F. M. Yanko, R. Balachandran, M. Aschner, A. B. Bowman, L. H. Nie, *Sci. Rep.* **2021**, *11*, 6385.
[195] E. M. Boon, D. M. Ceres, T. G. Drummond, M. G. Hill, J. K. Barton, *Nat. Biotechnol.* **2000**, *18*, 1096.

Elisabet Xifre-Perez received her Ph.D. (Hons.) degree in Electronics Engineering from the University Rovira i Virgili, Spain in 2007. She was a postdoctoral researcher at the Spanish National Research Council (CSIC) and at The Barcelona Institute of Science and Technology (ICFO) and doctoral researcher at the Ecole Polytechnique (France). She is currently a research fellow and lecturer at the Department of Electronic, Electric and Automatic Engineering of the University Rovira i Virgili. Her research work, developed at the Nanoelectronic and Photonic Systems group, focuses on the development and application of micro and nanoporous materials for biomedical and optoelectronic devices.

Josep Ferré-Borrull obtained his Physics degree in 1994, his B.Sc. in 1996 and his Ph.D. in 1998, all of them at the Universitat de Barcelona, where his Ph.D. research was concerned with optical image processing. His postdoctoral experience focused on surface nanoroughness characterization of high-quality optical components in the Fraunhofer Institute in Jena, Germany and in the ENEA in Rome, Italy. He joined the Universitat Rovira i Virgili in 2004 where his research is related to the development of technologies for nanoporous materials, their applications to energy, health and environment, and the numerical modeling of their interaction with the light.

Lluís F. Marsal is a distinguished professor and full professor at the Department of Electronic Engineering of the Universitat Rovira i Virgili, Spain. He was a postdoctoral researcher at the University of Waterloo, Ontario, Canada. He is a fellow of the Optical Society of America and received the ICREA Academia Award from the Generalitat of Catalunya. His research interests include porous silicon and nanoporous alumina for optical biosensing and biomedical applications and nanostructured materials to enhance light–matter interactions.